LONG-TERM EVALUATION OF THREE-DIMENSIONAL HELIOCENTRIC SOLAR SAIL TRAJECTORIES WITH ARBITRARY FIXED SAIL SETTING

J. C. VAN DER HA* and V. J. MODI**

The University of British Columbia, Vancouver, B.C., Canada

(Received 17 January, 1978)

Abstract. The solar radiation effects upon the orbital behaviour of an arbitrarily shaped spacecraft (or a solar sail in particular) in a general fixed orientation with respect to the local coordinate frame are investigated. Through introduction of a quasi-angle in the osculating plane, the motion of the orbital plane becomes uncoupled from the in-plane perturbations. Exact solutions in the form of conic sections and logarithmic spirals can readily be formulated for certain specific initial conditions. An effective out-of-plane spiral transfer trajectory is obtained by reversing the force component normal to the orbital plane at specified positions in the orbit. By choosing the appropriate control angles for the sail orientation, any point in space can be reached eventually. In the case of general initial conditions, the long-term orbital behaviour is assessed asymptotically by means of the two-variable expansion procedure. An implicit expression for the eccentricity is derived and explicit results are established by an iteration scheme. The other orbital elements can be expressed in terms of the eccentricity and their asymptotic series for near-circular initial orbits are also obtained.

While equations for the higher-order contributions as well as the periodic parts of their solutions can be formulated readily, their secular terms are determined only for a circular initial orbit.

List of Symbols

a	semi-major axis
a_e	semi-major axis of Earth's orbit, 1 A.U. = 1.496×10^8 km
$a^j{}_{nk}$, $b^j{}_{nk}$, $c^j{}_{nk}$, $d^j{}_{nk}$	slowly varying Fourier coefficients, Appendix II
c_s	constant in spiral trajectory, $-u'(\nu)/u(\nu)$
c_t	constant, Equation (9)
e	eccentricity
e_f, e_b	emissivities of front, and back side of surface element
e_p	modified eccentricity $[e^2{}_{00} + 2\varepsilon_s p_{00} R + \varepsilon_s{}^2 R^2]^{1/2}/(1 - \varepsilon_s R)$
$\mathbf{h}$	angular momentum (per unit mass) vector, $\mathbf{r} \times \mathbf{v}$
i	inclination of orbital plane with respect to ecliptic
l	semi-latus rectum
l_p	modified semi-latus rectum, $l_{00}/(1 - \varepsilon_s R)$
m	mass of satellite
n	number of illuminated surface components
p	auxiliary element, $e \cos \tilde{\omega}$
q	auxiliary element, $e \sin \tilde{\omega}$
$\mathbf{r}$	radius vector, pointing from origin to satellite, Figure 1
t	time (non-dimensional)

* Graduate Research Fellow, now at European Space Operations Centre, Darmstadt, F.R.G.
** Professor, Dept. of Mechanical Engineering.

Celestial Mechanics **19** (1979) 113–138. 0008–8714/79/0192–0113 $03.90.

u	inverse radius, $1/r$
$\mathbf{u}^n{}_k$	$(u^n{}_{kx}, u^n{}_{ky}, u^n{}_{kz})$, unit vector normal to surface component A_k with components along local coordinate axes
$\mathbf{u}_s$	$(u^s{}_x, u^s{}_y, u^s{}_z)$, unit vector along direction of radiation with components along local coordinate axes
w	auxiliary element, $1 - (1-e^2)^{1/2}$
A	total effective illuminated surface area of the satellite, cross-sectional area for spherical satellite
$A_0(\bar{\nu})$, $B_0(\bar{\nu})$	auxiliary functions in expression for M_0, Equation (21)
$A_j(\bar{\nu})$, $B_j(\bar{\nu})$	$(j = 2, 3, 4, 5)$ auxiliary functions in second-order results, Equation (41)
A_k	k-th surface component (non-dimensional)
A_{nk}, B_{nk}	$(n = 1, 2, \ldots ; k = 0, 1, 2, \ldots)$ integrals, defined and evaluated in Appendix I
B	auxiliary constant, $c_s T/(2S) = \varepsilon_s T/C$
C	constant in spiral trajectory, $u(\nu)l(\nu)$
$C_0(\bar{\nu})$	auxiliary function of $\bar{\nu}$, $(A^2{}_0 + B^2{}_0)^{1/2}$
$\mathbf{F} = (F_x, F_y, F_z)$	solar radiation force with components along local coordinate axes
K	component of $\mathbf{K}$ along orbit-normal
K_k	$K(\nu_k)$
$\mathbf{K}$	unit vector along Z-axis with components along local coordinate axes
L	component of $\mathbf{K}$ along local horizontal
M	component of $\mathbf{K}$ along local vertical
M_k	$M(\nu_k)$
R	component of $\mathbf{R}$ along local vertical
$\mathbf{R} = (R, S, T)$	functions of rotation angles α and β, and material properties, Equation (4) with components along local reference frame
S	component of $\mathbf{R}$ along local horizontal
S_c	solar constant, 1.35 kW m^{-2}
S'	solar radiation pressure, S_c/(velocity of light), 4.51×10^{-6} N m^{-2}
T	component of $\mathbf{R}$ along orbit-normal
T_f, T_b	temperature of front, and back side of surface element
$\mathbf{W}$	rotation vector, $\mathbf{w}^r + \dot{\mathbf{v}}$
X, Y, Z	inertial reference axes, Figure 1
$\alpha = (\alpha, \beta, \gamma)$	Eulerian control angles defining orientation of surface element with respect to orbital plane, Figure 1.
α_k, β_k	Eulerian control angles for surface component A_k
α_s	spiral angle, arctan (c_s)
ε_s	ratio of solar radiation and gravity forces for heliocentric orbits, $2S'\,(A/m)\,a^2{}_e/\mu_s = 1.52 \times 10^{-3}\,(A/m)$
κ	material parameter $(e_f T_f{}^4 - e_b T_b{}^4)/(e_f T_f{}^4 + e_b T_b{}^4)$
μ_s	Sun's gravitational parameter, 1.326×10^{20} m^3 s^{-2}
ν	quasi-angle in osculating plane, $\dot{\nu} = \dot{\phi} + \dot{\Omega}\cos(i)$, $\nu(0) = 0$, employed as independent variable
$\bar{\nu}$	slow independent variable, $\varepsilon_s \nu$
ν_k	$(k = 0, 1, 2, \ldots)$ abbreviation for $\nu_k = k\pi/(1 + B^2)^{1/2}$
ξ_0, η_0, ζ_0	reference axes, fixed to osculating plane in heliocentric orbits, ξ_0 along the local vertical, η_0 along the local horizontal and ζ_0 along the orbit-normal, Figure 1
ξ_1, η_1, ζ_1	intermediate frame of reference after rotation of solar sail by α, Figure 1
ξ, η, ζ	reference frame fixed to solar sail after rotations by α and β, Figure 1
ρ	material parameter characterizing specular reflectivity of surface component, $\rho_1\rho_2$
ρ_1	portion of incident photons which are reflected
ρ_2	portion of reflected photons which are reflected specularly
ρ_b, ρ_f	specular reflectivity for back and front side of surface element, respectively
ρ_k	specular reflectivity for surface component A_k

σ	material parameter for homogeneous flat plate, $\sigma_1 + \sigma_2 + \rho$, or homogeneous sphere, $(1 - \tau)/2 + 2\sigma_2/3$
σ_1, σ_2	material parameters, $\sigma_1 = (1 - \rho - \tau)/2$ and $\sigma_2 = [\rho_1(1 - \rho_2) + \kappa(1 - \rho_1 - \tau)]/3$
σ_{1k}, σ_{2k}	σ_1 and σ_2 for surface component A_k
τ	material parameter denoting transmissivity of surface element
ϕ	argument of latitude, i.e. position angle of satellite as measured from the line of nodes
ψ	angle characterizing shift of orbital plane, $\nu - \phi$
ω	argument of the perihelion with respect to the line of nodes
$\tilde{\omega}$	position of the perihelion measured in osculating plane from axis $\nu = 2\pi k$
$\tilde{\omega}_p$	modified position of the perihelion, arctan $[q_{00}/(p_{00} + \varepsilon_s R)]$
Ω	longitude of ascending node, measured from the autumnal equinox, Figure 1

Single subscripts refer to the order of the perturbation terms; 00 indicates initial conditions; dots and primes refer to differentiation with respect to time and ν, respectively.

1. Introduction

The steady flux of solar radiation in outer space offers an extremely attractive mode of propulsion (so-called solar sailing) for interplanetary space probes. The abundance of radiation energy ensures a reliable and unremitting source of motive power. In fact, for some deep-space missions, propulsion by solar radiation energy may well constitute the only foreseeable practical means of transfer. Since the magnitude of the thrust generated by the solar radiation pressure is proportional to the effective area/mass ratio of the spacecraft, it is imperative to employ the lightest materials available meeting the structural requirements for the sail and supporting booms. The combination of useful payload and solar sail would in most practical cases, lead to an area/mass ratio in the range of 50 to 200 $m^2\,(kg)^{-1}$ corresponding to characteristic accelerations between about 0.5 and 2 mm s^{-2}. A propellant force of this order of magnitude may be small in comparison with that from chemical thrusters, but the latter has a very limited lifetime. It is important, however, to utilize the available solar radiation power as efficiently as possible in order to limit the duration of the mission to a practical length of time. Instrumental in assessing the potential of the solar radiation force as a function of solar sail parameter and initial conditions would be a thorough understanding of the orbital behaviour under a fixed arbitrary sail setting with respect to the local coordinate frame.

Limiting the investigation to a planar trajectory, Tsu (1959) presented a solution in terms of a logarithmic spiral, while neglecting the radial component of the velocity. London (1960) remedied this shortcoming and determined, graphically, the best sail setting and corresponding spiral angle for minimum-time spiral transfer. The spiral trajectory solution, however, suffers from an unnatural constraint in the sense that only very specific initial conditions lead to this type of trajectories. Pozzi *et al.* (1961) suggested an iteration scheme to accommodate more general initial conditions. This procedure was initiated by postulating an approximate expression for the tangential velocity. A fairly extensive survey of solar sail trajectories and a feasibility study of various missions were presented by Kiefer (1965).

Wesseling (1967) studied solar-powered low-thrust trajectories in the vicinity of the ecliptic plane, using a perturbation approach with the spiral trajectory as a first approximation. More recently, Modi *et al.* (1973) suggested an on–off strategy where during the on-phase the sail is kept normal to the radiation, leading to a significant elongation of the orbit as the perihelion moves towards and the aphelion away from the Sun.

Analytical long-term valid solutions for solar radiation induced orbital perturbations in a geocentric ecliptic orbit were given by Van der Ha and Modi (1977). In the present analysis, a constant component of the force normal to the instantaneous orbital plane is also taken into account. In this situation, an exact solution can still be formulated in terms of a logarithmic spiral by separating the in-plane from the out-of-plane motion.

When the out-of-plane component of the thrust is kept constant throughout, the orbital plane itself will exhibit a wobbling motion, returning to its original orientation in slightly less than one revolution. An effective out-of-plane transfer trajectory is presented involving the reversal of the out-of-plane force-component at specified positions in the orbit. By choosing the appropriate control angles for the sail orientation, any point in the solar system can be reached eventually by this three-dimensional spiral trajectory.

Taking a homogeneous solar sail with arbitrary reflecting characteristics, asymptotic representations in terms of ε_s (ratio of solar radiation and gravity forces) are determined for the optimal sail setting and corresponding spiral angle, maximizing the radial distance as a function of time.

Whereas a specific initial velocity vector is required for embarking upon the spiral trajectory, other trajectories emanating from different initial conditions may also be of interest. Therefore, a three-dimensional short-term solution is presented for arbitrary initial conditions. Subsequently, a long-term analysis by means of the two-variable expansion procedure is presented, yielding an implicit equation for the long-term behaviour of the eccentricity. By iteration, the solution may be determined up to the desired accuracy. For not too large values of initial eccentricity, asympotic expansions up to order e^5 should be useful. The other orbital elements can be expressed in terms of the eccentricity and can be calculated up to the required accuracy. Higher-order terms may become of importance when the area over mass ratio of the sail is large. Equations for the higher-order terms can be derived and solved for their periodic parts. The higher-order secular terms, however, are hard to determine analytically, but the order of magnitude of their contributions can be estimated.

2. Formulation of the Problem

An inertial X, Y, Z reference frame with origin at the center of the sun is introduced in Figure 1(a) where the X axis points to the initial position of the spacecraft and the X, Y plane constitutes the initial osculating plane, usually the ecliptic. The Z axis is aligned with the initial angular momentum vector. In addition, a local ξ_0, η_0, ζ_0

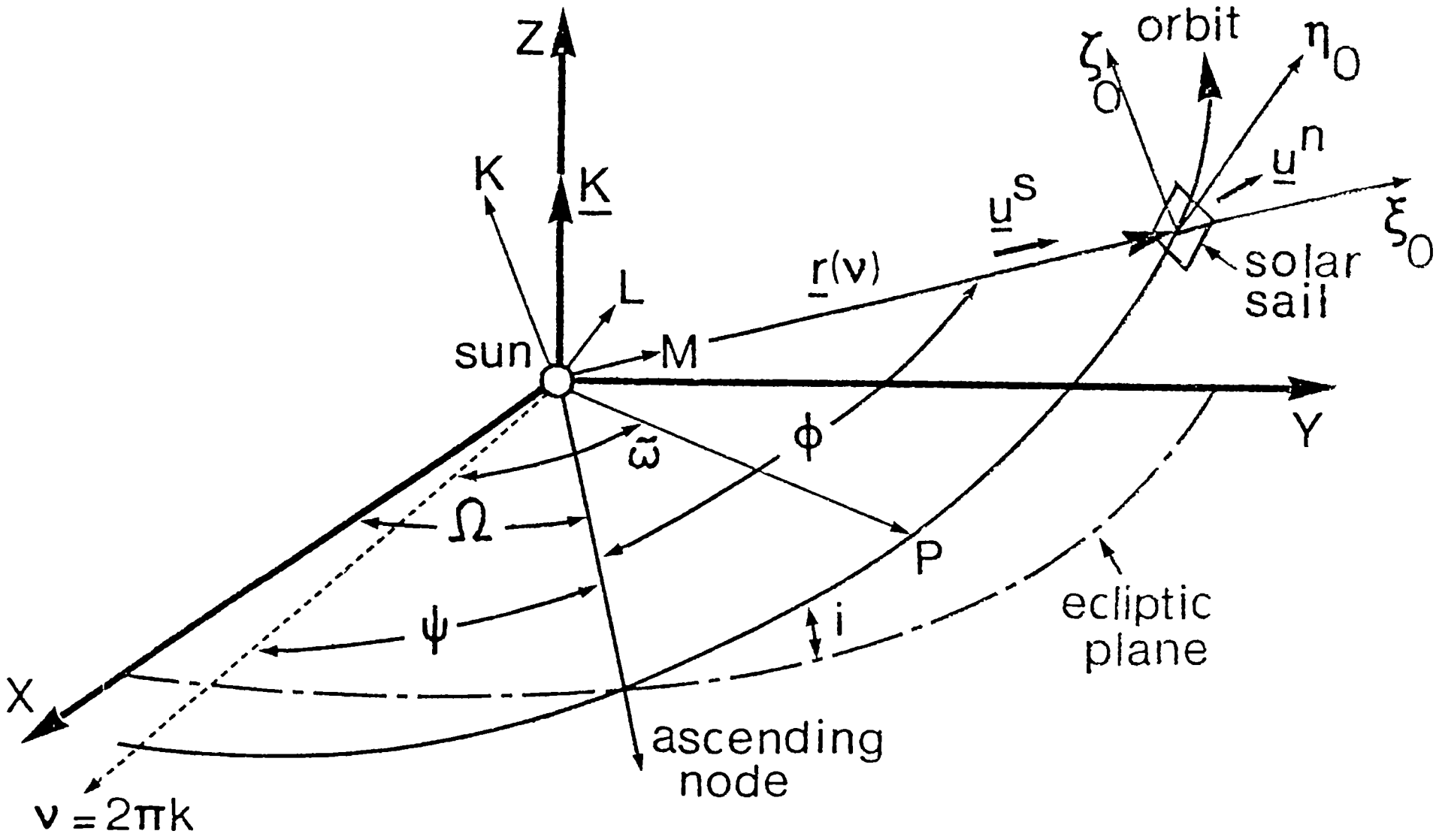

[a] $\nu = \phi + \psi$

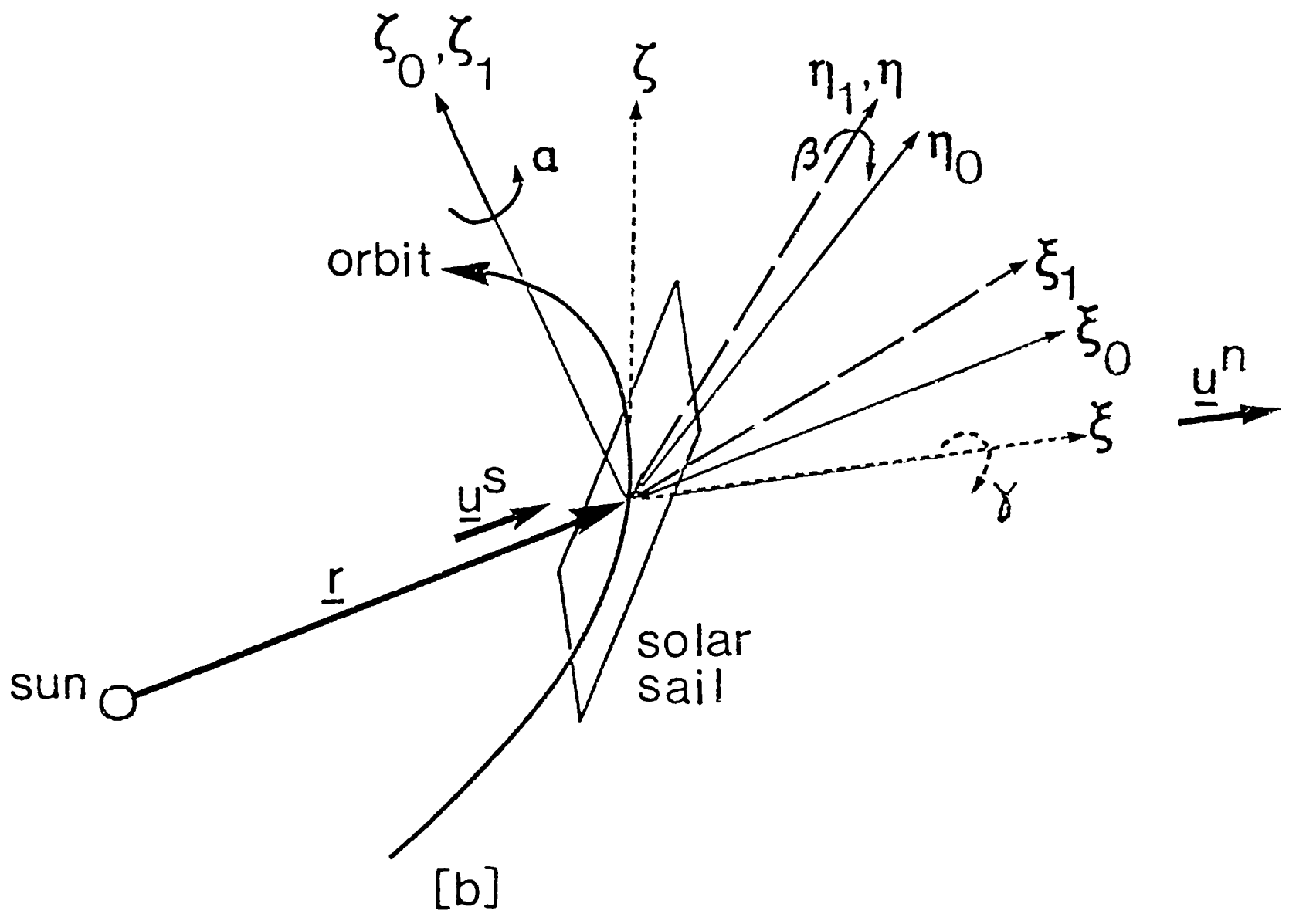

[b]

Fig. 1. (a) Configuration of the sun and solar sail in a heliocentric trajectory; (b) Successive rotations α, β and γ for defining arbitrary orientation of solar sail.

reference frame moving along with the spacecraft is introduced: the ξ_0, η_0 and ζ_0 axes point along the local vertical, local horizontal and orbit-normal directions, respectively. Any desired orientation of the solar sail in the ξ_0, η_0, ζ_0 can be described

by three successive Eulerian rotations (Figure 1(b)). Taking, initially, the outward normal to the sail to be directed along the ξ_0 axis, a first rotation α about the ζ_0 axis produces the ξ_1, η_1, ζ_1 frame and brings the solar sail to the required line of intersection with the orbital plane. A subsequent rotation β about the η_1 axis yields the ξ, η, ζ frame and moves the normal to the sail out of the orbital plane to its prescribed orientation. A final rotation γ about the normal (ξ axis) could be performed for attaining the proper attitude of the sail in its η, ζ plane without affecting the solar radiation force. The components of $\mathbf{u}^n$ taken along the local ξ_0, η_0, ζ_0 axes depend on α and β only:

$$\mathbf{u}^n = (\cos\alpha\cos\beta, \sin\alpha\cos\beta, -\sin\beta). \tag{1}$$

For many satellites, solar panels form a substantial portion of the total surface area. This would particularly be so for a spacecraft designed to be propelled by solar radiation pressure. Hence, in these situations, only the area of solar panels or sails needs to be considered. In general, the spacecraft is modelled by a number of surface components, characterized by their own material parameters and orientation. In nondimensional form (unit of length equals $a_e = 1$ A.U. and unit of time is $1/(2\pi)$ year), the solar radiation force upon an arbitrary space structure of homogeneous, illuminated surface components A_k, $k = 1, 2, \ldots, n$ in an heliocentric orbit is written as

$$\mathbf{F} = \varepsilon_s \sum_{k=1}^{n} |\mathbf{u}_k^n \cdot \mathbf{u}^s| \{\sigma_{1k}\mathbf{u}^s + [\sigma_{2k} + \rho_k(\mathbf{u}_k^n \cdot \mathbf{u}^s)]\mathbf{u}_k^n\} A_k/r^2, \tag{2}$$

where the physical force is nondimensionalized through multiplication by $a_e^2/(\mu_s m)$. The small parameter ε_s denotes the ratio of solar radiation and attraction forces,

$$\varepsilon_s = 2S'(A/m)(a_e^2/\mu_s) = 1.57 \times 10^{-3}\,(A/m).$$

It should be mentioned that the solar radiation pressure S' is defined as the quotient of the solar constant (i.e. energy incident per unit time and unit normal area at $a_e = 1$ A.U. from the sun, 1.35 kW m^{-2}) and the velocity of light. Note that the solar constant and hence the radiation force in Equation (2) varies inversely as square of the distance from the sun. This is because the total radiant energy emitted by the sun in a given time equals that passing through any concentric spherical surface around the sun in that time (taking the rate of energy output constant). The material parameters σ_1, σ_2 and ρ are defined as follows.

$$\sigma_1 = (1 - \rho - \tau)2,$$

$$\sigma_2 = [\rho_1(1 - \rho_2) + \kappa(1 - \rho_1 - \tau)/3] \operatorname{sign}(\mathbf{u}^n \cdot \mathbf{u}^s),$$

$$\rho = \rho_1\rho_2,$$

where ρ_1 denotes the total portion of incident photons which are reflected and ρ_2 the fraction which is reflected specularly. The parameter κ depends on the emissivities and temperatures of the front and back sides of the surface:

$$\kappa = (e_f T_f^4 - e_b T_b^4)/(e_f T_f^4 + e_b T_b^4).$$

The unit-vectors $\mathbf{u}^s$ and $\mathbf{u}_k^n$ point in the direction of the radiation and along the normal to the surface component A_k, respectively.

Writing $\mathbf{F} = \varepsilon_s \mathbf{R}/r^2$ with auxiliary vector $\mathbf{R} = (R, S, T)$ the components of $\mathbf{R}$ can be evaluated for an arbitrarily shaped spacecraft using Equation (2):

$$R = \sum_{k=1}^{n} \cos\alpha_k \cos\beta_k \{\sigma_{1k} + [\sigma_{2k} + \rho_k \cos\alpha_k \cos\beta_k] \cos\alpha_k \cos\beta_k\} A_k;$$

$$S = \sum_{k=1}^{n} \sin\alpha_k \cos\alpha_k \cos^2\beta_k [\sigma_{2k} + \rho_k \cos\alpha_k \cos\beta_k] A_k;$$

$$T = -\sum_{k=1}^{n} \cos\alpha_k \cos\beta_k \sin\beta_k [\sigma_{2k} + \rho_k \cos\alpha_k \cos\beta_k] A_k.$$

The normal $\mathbf{u}_k^n$ to a surface element A_k, $k = 1, 2, \ldots, n$ is taken in such a manner that its projection along the radiation is always positive.

In general, when $T \neq 0$, the plane of the orbit will shift. The motion of the ξ_0, η_0, ζ_0 frame relative to the inertial X, Y, Z frame may be described in terms of the rotation vector $\mathbf{W}$ with components W_1, W_2, W_3 along the instantaneous ξ_0, η_0, ζ_0 axes:

$$\mathbf{W} = \begin{bmatrix} W_1 \\ W_2 \\ W_3 \end{bmatrix} = \begin{bmatrix} \dot{\Omega} \sin\phi \sin(i) + \dot{(i)} \cos\phi \\ \dot{\Omega} \cos\phi \sin(i) - \dot{(i)} \sin\phi \\ \dot{\nu} = \dot{\phi} + \dot{\Omega} \cos(i) \end{bmatrix} \tag{3}$$

Since the velocity vector $\dot{\mathbf{r}}$ lies in the instantaneous orbital (ξ_0, η_0) plane (condition of osculation), the vector $\mathbf{W} \times \mathbf{r}$ cannot have a component along the ζ_0 axis, implying that $W_2 = 0$. The motion of the ξ_0, η_0, ζ_0 reference frame can be visualized as the sum of the rotations $W_3 = \dot{\nu}$ along the normal and W_1 along the radial directions, the latter component solely describing the shift in the orientation of the orbital plane. The equations of motion follow from Newton's second law, accounting for rotation, with scalar components along the ξ_0, η_0, ζ_0 axes given as:

$$\begin{aligned} \ddot{r} + 1/r^2 - r\dot{\nu}^2 &= \varepsilon_s R/r^2, \\ r\dot{\nu} + 2\dot{r}\dot{\nu} &= \varepsilon_s S/r^2, \\ rW_1\dot{\nu} &= \varepsilon_s T/r^2. \end{aligned} \tag{4}$$

The characteristic feature of this formulation is the fact that the in-plane perturbations appear uncoupled from the out-of-plane force component. It is advantageous to employ the quasi-angle ν, Equation (3), as the independent variable. It is emphasized that ν is measured from a fixed line in the osculating plane and its dependence on time is given by

$$\dot{\nu} = \dot{\phi} + \dot{\Omega} \cos(i) = l^{1/2}/r^2,$$

which can be derived from angular momentum considerations ($h = l^{1/2}$) in con-

junction with the last relation of Equations (3). As in the case of the classical Keplerian solution, the in-plane equations can be transformed in terms of the inverse radius $u = 1/r$ and the semi-latus rectum l. As to the orientation of the orbital plane, $\Omega'(\nu)$ contains a singularity for $i = 0$ so that a formulation in terms of the unit-vector **K** directed along the inertial Z axis with components $M = \sin(i)\sin(\nu - \psi)$, $L = \sin(i)\cos(\nu - \psi)$ and $K = \cos(i)$ along the local ξ_0, η_0, ζ_0 axes is favoured. As the local ξ_0, η_0, ζ_0 frame moves along with the spacecraft in its orbit, the vector $\mathbf{K}(\nu)$ traces a path upon the sphere $(\mathbf{K}\cdot\mathbf{K}) = 1$ in the ξ_0, η_0, ζ_0 frame. The orbital inclination i and the angle $\psi = \nu - \phi$, characterizing the shift in the orbital plane (Figure 1(a)) can be determined quite readily from the vector **K**. The complete system of equations is written as:

$$
\begin{aligned}
&u''(\nu) + u(\nu) = (1 - \varepsilon_s R)/l(\nu) - \varepsilon_s S u'(\nu)/[u(\nu)l(\nu)];\\
&l'(\nu) = 2\varepsilon_s S/u(\nu);\\
&M''(\nu) + M(\nu) = \varepsilon_s T K(\nu)/[u(\nu)l(\nu)];\\
&K'(\nu) = -\varepsilon_s T M'(\nu)/[u(\nu)l(\nu)].
\end{aligned}
\tag{5}
$$

The first two equations fully describe the in-plane perturbations and the latter two equations define the orientation of the osculating plane. The component $L(\nu)$ can be shown to be equal to $M'(\nu)$. The initial conditions for the system of Equations (5) are written as $l(0) = l_{00}$; $u(0) = (1 + e_{00}\cos\tilde{\omega}_{00})/l_{00}$; $u'(0) = (e_{00}\sin\tilde{\omega}/l_{00}$; $K(0) = 1$ and $M(0) = M'(0) = 0$.

In a few particular situations, exact solutions for the system of Equations (5) can be established: in the case where the component S vanishes (e.g., when the normal to the solar sail lies in the ξ_0, ζ_0 plane or when all of the radiation is absorbed), solutions for the orbital motion can be obtained using the classical Keplerian procedure. After modification of the sun's gravitational parameter to account for the apparent reduction in attraction because of the solar radiation force, the trajectory for the case $S = 0$ can be written as $u(\nu) = [1 + e_p\cos(\nu - \tilde{\omega}_p)]/l_p$ with modified orbital elements $l_p = l_{00}/(1 - \varepsilon_s R)$, $e_p = [e_{00}^2 + 2\varepsilon_s p_{00} R + \varepsilon_s^2 R^2]^{1/2}/(1 - \varepsilon_s R)$ and $\tilde{\omega}_p = \arctan[q_{00}/(p_{00} + \varepsilon_s R)]$, where all angles are measured in the osculating plane. Another, more interesting, exact solution arises when the initial velocity vector satisfies a prescribed condition leading to a trajectory in the shape of a logarithmic spiral.

3. Three Dimensional Spiral Trajectories

The spiral trajectory of the form $r(\nu) = r_{00}\exp(c_s\nu)$ emerges from Equations (5) when one looks for solutions having the properties that the product $u(\nu)l(\nu)$ remains constant, say C, and $u'(\nu) = -c_s u(\nu)$ at all times. The constants c_s and C can be

evaluated from Equations (5) after substitution of these two relations:

$$\begin{aligned} c_s &= \{(1 - \varepsilon_s R) - [(1 - \varepsilon_s R)^2 - 8\varepsilon_s^2 S^2]^{1/2}\}/(2\varepsilon_s S) \\ &= 2\varepsilon_s S\{1 + \varepsilon_s R + \varepsilon_s^2(R^2 + 2S^2) + \varepsilon_s^3 R(R^2 + 6S^2)\} + 0(\varepsilon_s^5); \\ C &= 2\varepsilon_s S/c_s = (1 - \varepsilon_s R)\{1 - 2\varepsilon_s^2 S^2[1 + \varepsilon_s R + \varepsilon_s^2(R^2 + 2S^2)]\} + \\ &\quad + 0(\varepsilon_s^5). \end{aligned} \tag{6}$$

Taking $r(0) = r_{00}$, the complete in-plane and out-of-plane solutions of Equations (5) can be expressed in terms of c_s and C:

$$\begin{aligned} r(\nu) &= r_{00} \exp(c_s \nu); \\ l(\nu) &= Cr(\nu); \\ M(\nu) &= B\{1 - \cos[(1 + B^2)^{1/2}\nu]\}/(1 + B^2); \\ L(\nu) &= B \sin[(1 + B^2)^{1/2}\nu]/(1 + B^2)^{1/2}; \\ K(\nu) &= \{1 + B^2 \cos[(1 + B^2)^{1/2}\nu]\}/(1 + B^2). \end{aligned} \tag{7}$$

Here the constant B stands for $\varepsilon_s T/C$. It is seen that the radial distance takes the form of a logarithmic spiral (outward if $S > 0$ and inward for $S < 0$), while the orbital plane exhibits a periodic wobbling motion with maximum inclination at $\nu = \pi/(1 + B^2)^{1/2}$. This is of practical interest for a solar sail since it predicts that no secular changes in the orbital orientation are induced by a constant force component normal to the plane of the orbit.

It must be emphasized that the spiral trajectory arises only when the spacecraft possesses the right velocity vector at injection. Its radial and circumferential components are given by $\dot{r} = c_s(C/r)^{1/2}$, $r\dot{\nu} = (C/r)^{1/2}$, and the spiral angle α_s equals arctan (c_s). Additional insight into the nature of the trajectory is provided by studying the osculating ellipses of the spiral. The eccentricity and perigee position at any point ν_1 are given by

$$\begin{aligned} e_1 &= [c_s^2 \exp(-2c_s\nu_1) + (1 - C)^2]^{1/2}, \\ \tilde{\omega}_1 &= \nu_1 - \pi + \arctan[c_s \exp(-c_s\nu_1)/(1 - C)], \end{aligned} \tag{8}$$

so that the equation for the osculating ellipse at $\nu = \nu_1$ can be written as $r(\nu_1) = C \exp(c_s\nu_1)/[1 + e_1 \cos(\nu_1 - \tilde{\omega}_1)]$. It is of interest to note that the eccentricity which is of the order ε_s to start with, decreases slowly attaining the limiting value $\varepsilon_s R + 0(\varepsilon_s^2)$ as $\nu_1 \to \infty$. This is of considerable importance since it predicts that a space-probe can be released from a spiral solar sail trajectory into a near-circular heliocentric orbit at any time. As to the position of the perigee of the osculating ellipses, it follows that $\tilde{\omega}_1$ follows ν_1 steadily, lagging behind by an angle of between $\pi/2$ and π radians in case $S > 0$ and between π and $3\pi/2$ radians if $S < 0$. As the spacecraft moves along its trajectory, the angle between the radius vector and oscu-

lating perigee will increase (for $S > 0$) or decrease ($S < 0$) slowly until, finally, $\tilde{\omega}_1 \to \nu_1 - \pi$ for $\nu_1 \to \infty$.

An explicit expression in terms of the solar sail parameters can be obtained for the time history in the spiral trajectory,

$$t(\nu) = \int_0^{\nu} [r^2(\tau)/l^{1/2}(\tau)]\, \mathrm{d}\tau = r_{00}^{3/2}[\exp(3c_s\nu/2) - 1]/c_t,$$

with

$$c_t = 3 \operatorname{sign}(S)/2\{1 - \varepsilon_s R) - [(1 - \varepsilon_s R)^2 - 8\varepsilon_s^2 S^2]^{1/2}\}^{1/2}. \tag{9}$$

The radial distance as a function of time follows by combining Equations (7) and (9).

$$r(t) = r_{00}(1 + c_t t/r_{00}^{3/2})^{2/3}. \tag{10}$$

This result is valid for both outward ($S > 0$) and inward ($S < 0$) spirals.

To obtain the most favourable sail setting for reaching the maximum radial distance at any time t, the coefficient c_t is maximized as a function of the rotation angles α and β. It follows that the maximum occurs when β vanishes, producing a planar trajectory. The value of α is determined from

$$8\varepsilon_s S\frac{\partial S}{\partial \alpha} + \{(1 - \varepsilon_s R) - [(1 - \varepsilon_s R)^2 - 8\varepsilon_s^2 S^2]^{1/2}\}\frac{\partial R}{\partial \alpha} = 0. \tag{11}$$

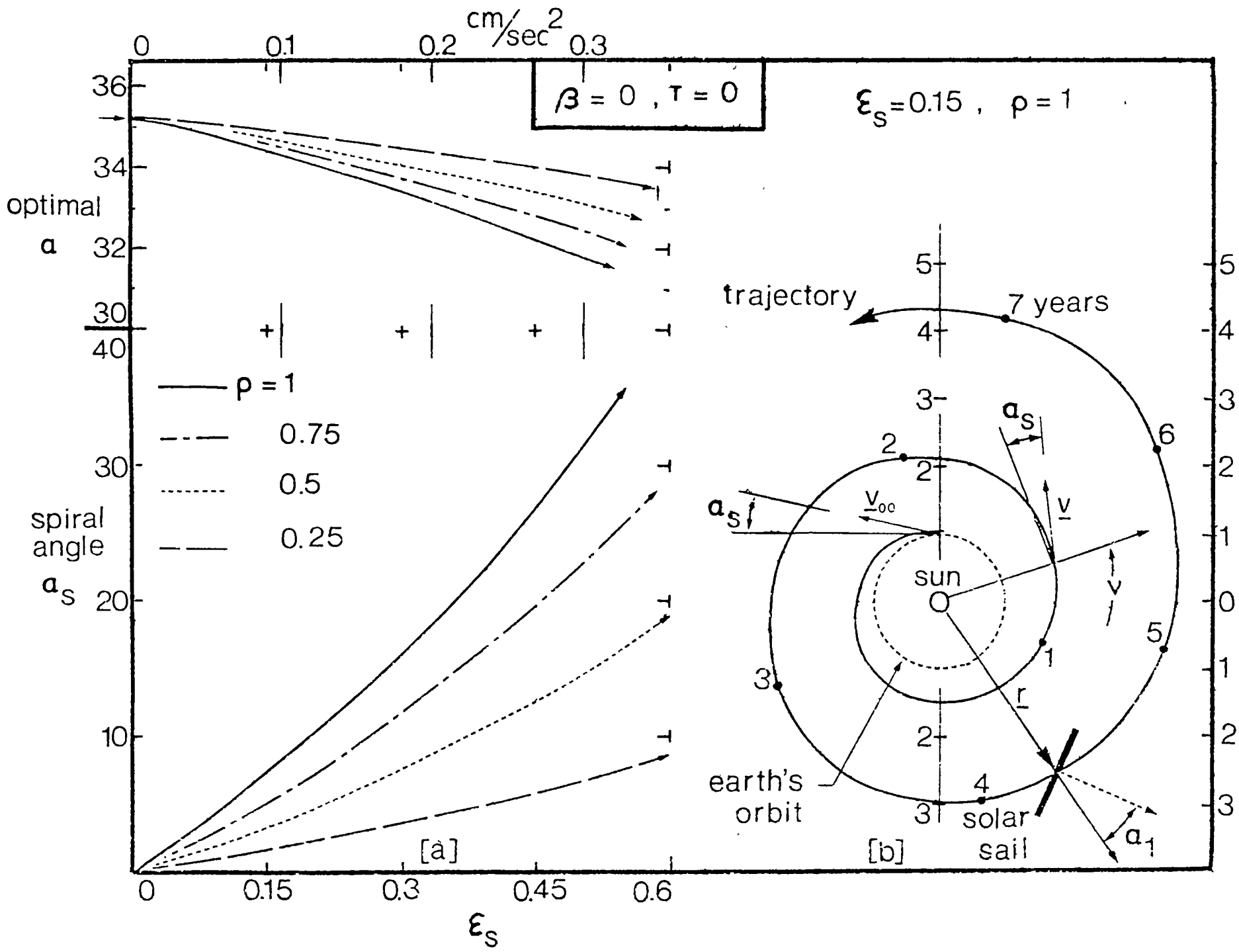

Fig. 2. (a) Optimal sail orientation and corresponding spiral angle for various values of reflectivity; (b) Actual planar spiral trajectory for $\varepsilon_s = 0.15$ and $\rho = 1$.

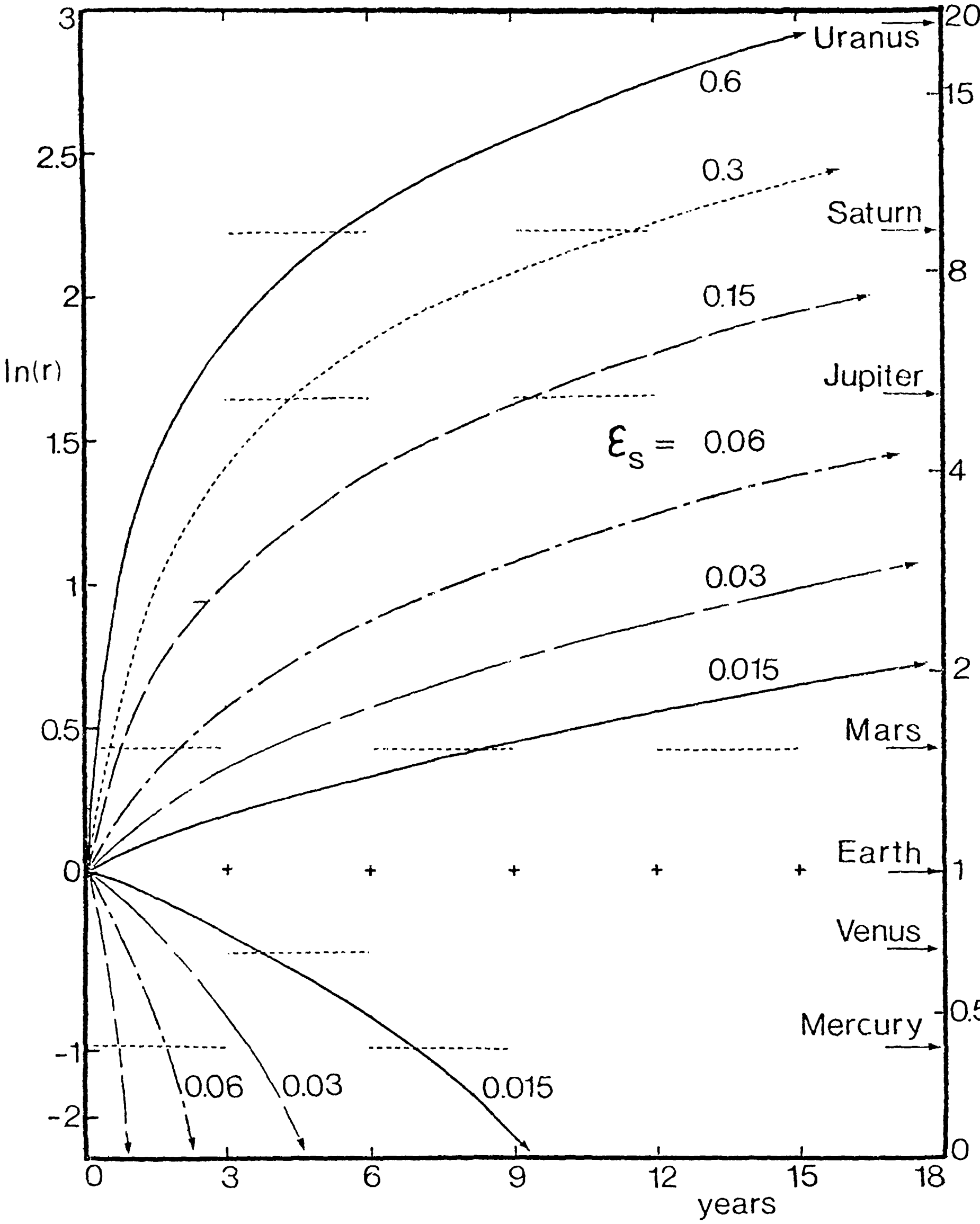

Fig. 3. Potential for near-circular interplanetary transfer by solar sail for a few values of ε_s.

Since the exact solution of this implicit equation for α cannot easily be found, it is useful to determine subsequent levels of approximation for α written as an asymptotic series in the small parameter ε_s: $\alpha = \alpha_0 + \varepsilon_s\alpha_1 + \varepsilon_s^2\alpha_2 + \ldots$. The equations for α_1, $i = 0, 1, 2, \ldots$, can be derived by substituting the series into Equation (11), developing the relation in terms of a Taylor expansion around $\alpha = \alpha_0$ and requiring that all coefficients of ϵ_s^n, $n = 0, 1, 2, \ldots$, vanish. After a considerable amount of algebra, the following asymptotic representation for α is found (taking a sail with

$\sigma_2 = 0$):

$$\alpha = \arcsin(3^{-1/2}) - \varepsilon_s 3^{1/2}(\sigma_1 + 2\rho)/36 - \varepsilon_s^2 2^{1/2} \times \\ \times (\sigma_1 + 2\rho)(5\rho + 43\sigma/6)/288 - \varepsilon_s^3 3^{1/2}(\sigma_1 + 2\rho)/2 \times \\ \times \{1261\sigma_1^2 + 1252\rho^2 + 1588\rho\sigma_1 + 72\sigma_1 + 144\rho\}/(36)^3 + 0(\varepsilon_s^4). \quad (12)$$

Subsequently, an explicit relation for the spiral angle α_s corresponding to the optimal orientation is found by substituting the optimal angle into c_s, Equations (6). Expansion for small ε_s yields:

$$\alpha_s = 4\rho\varepsilon_s 3^{1/2}/9\{1 + 6^{1/2}\varepsilon_s(\sigma_1 + 2\rho/3)/3 + \\ + \varepsilon_s^2[(\sigma_1 + 2\rho)^2/48 + 2(\sigma_1 + 2\rho/3)^2/3 + 8\rho^2/81]\} + 0(\varepsilon_s^4). \quad (13)$$

In Figure 2(a), the optimal orientation of the solar sail as well as the corresponding spiral angle have been plotted for various values of the reflectivity ρ. For low values of ε_s, the optimal orientation can be taken as 35.26°. It is evident that the spiral angle approaches zero for $\rho \to 0$ since the case $\rho = 0$ corresponds to a closed trajectory. Figure 2(b) illustrates an example of a planar spiral trajectory, showing the spiral angle and the orientation of the sail. The value of ε_s taken here (0.15) would correspond to A/m of about 100 m^2 $(kg)^{-1}$.

It is interesting to calculate the optimal radial distance over a long duration of time, showing the effectiveness of the spiral trajectory in near-circular orbital transfer, for a few values of the solar parameter ε_s. The results are summarized in Figure 3 for both inward and outward spirals. In case $\varepsilon_s = 0.015$, i.e. $A/m = 10\ m^2/(kg)^{-1}$, the orbit of Mars could be reached within 9 years and Venus in 4 years. For higher

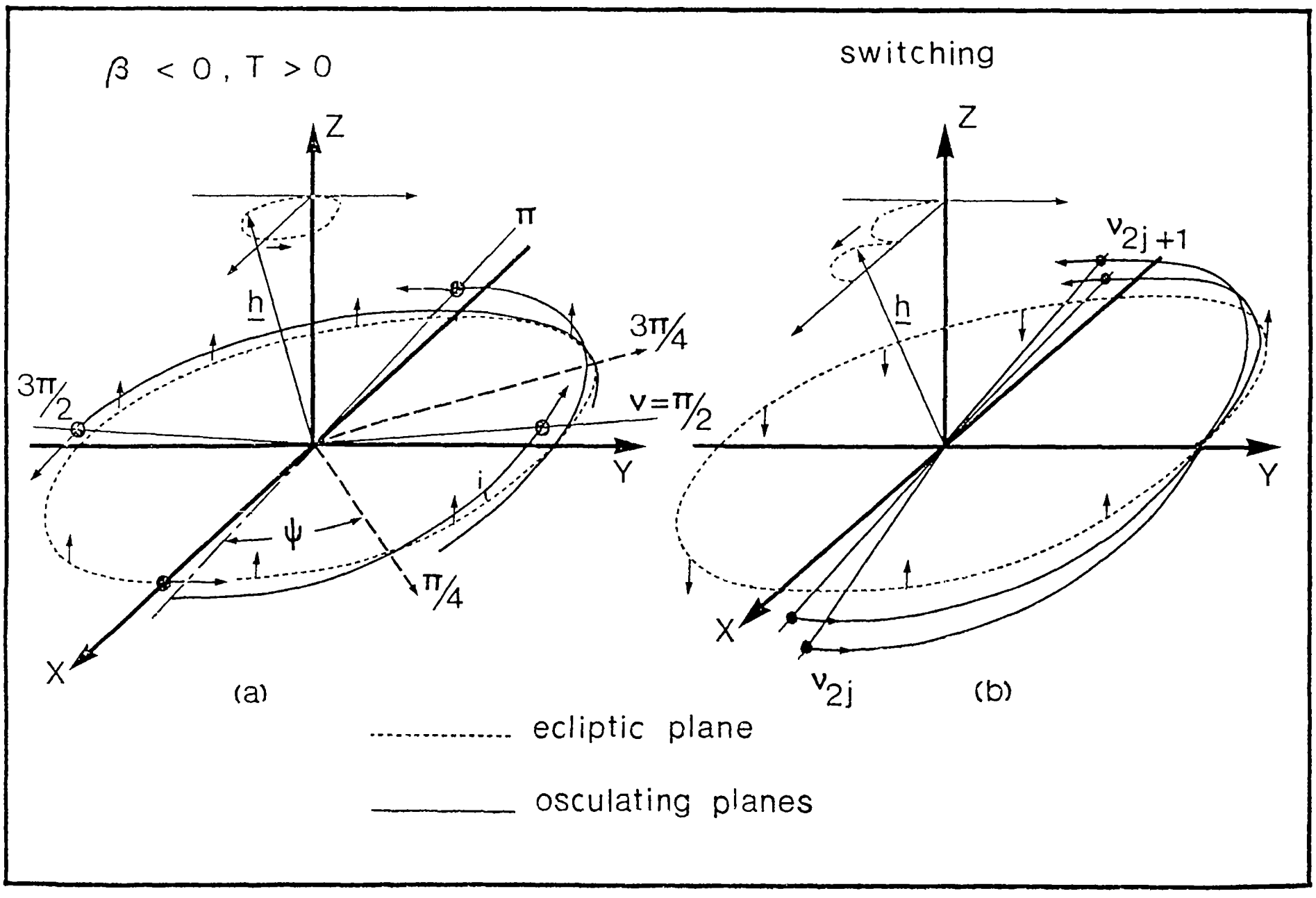

Fig. 4. (a) Orientation of the osculating plane as affected by a constant force normal to it; (b) Switching strategy leading to a systematic increase in orbital inclination.

values of ε_s the opportunities increase rapidly: even a long journey to the distant planet Uranus may be feasible if a solar sail with A/m of the order of 400 m^2 $(kg)^{-1}$ could be constructed.

The analysis remains valid when the component T of the force is non-zero: the position and velocity vectors of the spiral trajectory lie in the osculating plane in that case. The orientation of the orbital plane described by the angles i and ψ follows from Equations (7):

$$\begin{aligned} i(\nu) &= \arccos\{1 - 2B^2 \sin^2[(1 + B^2)^{1/2}\nu/2]/(1 + B^2)\}; \\ \psi(\nu) &= \nu - \arctan\{\tan[(1 + B^2)^{1/2}\nu/2]/(1 + B^2)^{1/2}\}. \end{aligned} \tag{14}$$

Expansion of $\psi(\nu)$ for small ε_s leads to $\psi(\nu) = \nu/2 + 0(\varepsilon_s^2), 0 \leq \nu \leq 2\pi$, so that the line of nodes precesses at approximately half the orbital rate. The inclination reaches its maximum at $\nu = \pi/(1 + B^2)^{1/2}$ and returns to zero at $2\pi/(1 + B^2)^{1/2}$, while $\psi(\nu)$ shows a discontinuity of π radians at $\nu = 2\pi/(1 + B^2)^{1/2}$. Figure 4(a) shows the orientation of the osculating plane at a few points in the orbit.

4. Out-of-Plane Spiral Transfer

In order to obtain a net increase in inclination after one revolution, the orientation of the sail would have to be changed during the orbit. Obvious switching points would be the instants when $i(\nu)$ is stationary, i.e., at $\nu_1 = \pi/(1 + B^2)^{1/2}$ and $\nu_2 = 2\nu_1$. Assuming the switching to take place instantaneously from $-\beta$ to $+\beta$ (without affecting the control angle α) and repeating the procedure during each subsequent revolution, the out-of-plane component T becomes

$$T = \begin{cases} |T|, \beta < 0; & \nu_{2j} < \nu < \nu_{2j+1}; \\ -|T|, \beta > 0; & \nu_{2j+1} < \nu < \nu_{2j+2}; \end{cases} \tag{15}$$

for $j = 0, 1, 2, \ldots$, and the switching points $\nu_k = k\pi/(1 + B^2)^{1/2}$, $k = 0, 1, 2, \ldots$. Since the operation takes place instantaneously, the force components S and R remain unchanged throughout. Writing $M_k = M(\nu_k)$ and $K_k = K(\nu_k)$, etc., $k = 0, 1, 2, \ldots$, the solution $i(\nu)$ is found by repeated application of the results in Equations (7):

$$i(\nu) = \begin{cases} \arccos\{K_{2j} + |B|(M_{2j} - |B|K_{2j})(1 - \cos[(1 + B^2)^{1/2}\nu])/(1 + B^2)\}, \\ \arccos\{K_{2j} + 2|B|(M_{2j} - |B|K_{2j})/(1 + B^2) - |B|[(3B^2 - 1)M_{2j} + \\ \qquad + |B|(3 - B^2)K_{2j}](1 + \cos[(1 + B^2)^{1/2}\nu])/(1 + B^2)^2\}, \end{cases} \tag{16}$$

where the former relation holds for $\nu_{2j} < \nu < \nu_{2j+1}$ and the latter for $\nu_{2j+1} < \nu < \nu_{2j+2}$. The following recurrence relations for K_{2j} and M_{2j} can be established:

$$\begin{aligned} M_{2j} &= -\{4|B|(1 - B^2)K_{2j-2} + [4B^2 - (1 - B^2)^2]M_{2j-2}\}/(1 + B^2)^2, \\ K_{2j} &= -\{[4B^2 - (1 - B^2)^2]K_{2j-2} - 4|B|(1 - B^2)M_{2j-2}\}/(1 + B^2)^2, \end{aligned} \tag{17}$$

with $j = 1, 2, 3, \ldots$ and $M_0 = 0$, $K_0 = 1$. A long-term linear approximation for $i(\nu)$, $i(\nu) = 2\varepsilon_s|T|(1 + B^2)^{1/2}\nu/\pi$, provides a good estimate as long as ε_s is sufficiently

small. The line of nodes, i.e., the intersection of the instantaneous orbital plane and the X, Y plane is located at $\nu = \nu_1 - \pi/2 = \pi/2 + 0(\varepsilon_s)$ when the first switching takes place. It returns to this position at all switching points while slightly deviating from this line in between. Through Equation (9), the switching instants are also known in terms of time.

The foregoing analysis is valid for any fixed sail orientation designated by the control angles α and β. Since the rate of increase in inclination is proportional to the magnitude of the force component $|T|$, the most effective (fixed angle) strategy is the one which maximizes $|T|$, i.e., $\alpha = 0$ and $|\beta| = \arcsin(3^{-1/2}) = 35.26°$. In this case $S = 0$ and the trajectory is a degenerate spiral maintaining a constant distance from the sun (so-called 'cranking orbit'). The behaviour of the inclination for this case is illustrated in Figure 5(c) for a few values of ε_s. While it would take about 14 years to make a full 180° swing through space at 1 A.U. from the sun, the duration would be less than 5 years at 0.5 A.U. (taking $\varepsilon_s = 0.15$).

An obvious application of three-dimensional spiral trajectories in conjunction with switching would be in a transfer mission where both inclination and radial distance are to be changed. From this consideration, it would be interesting to determine the most efficient orientation of the sail for a near-circular out-of-plane transfer with the final radial distance prescribed and the inclination to be maximized

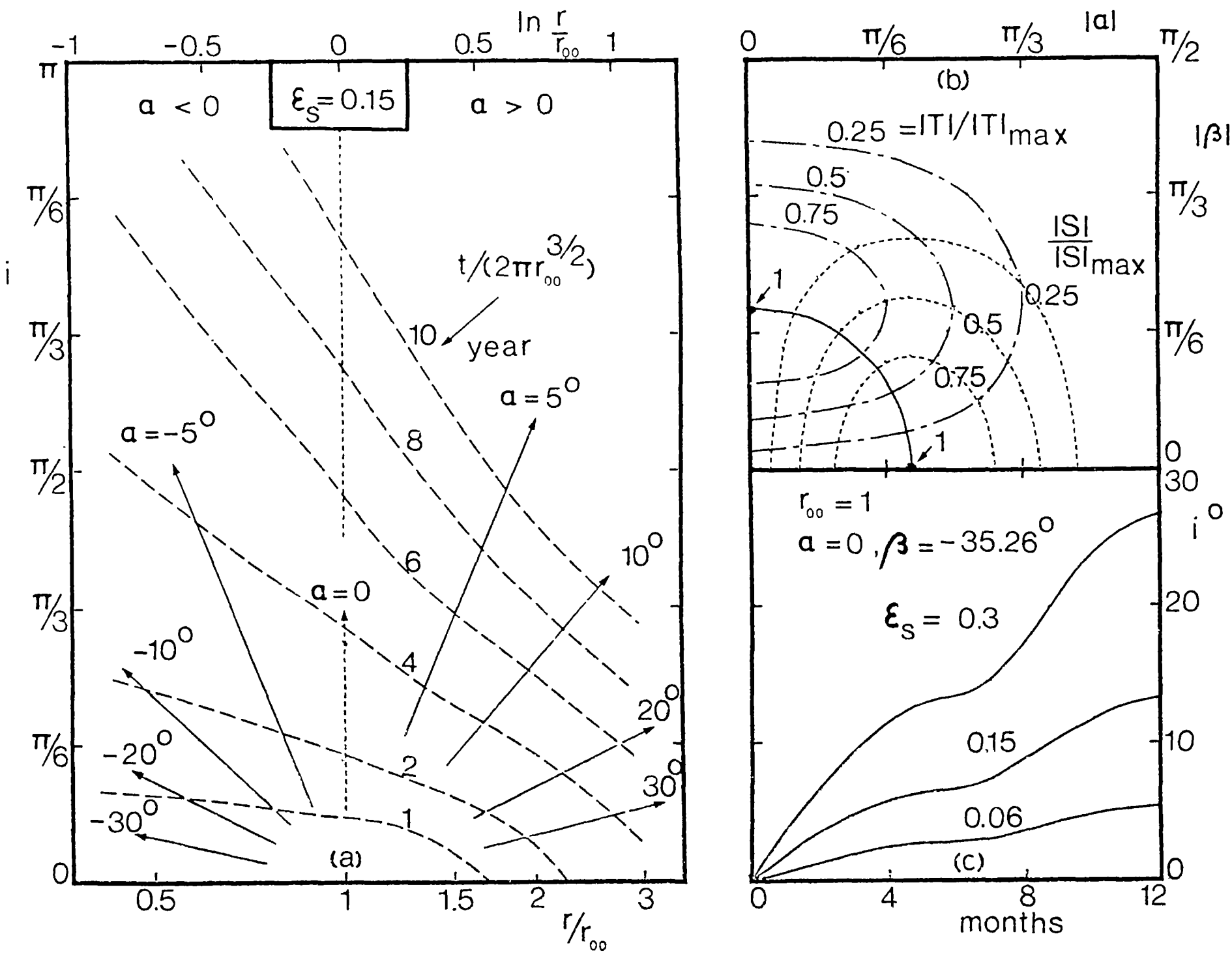

Fig. 5. (a) Combinations of inclination and radial distance attainable after a given time; (b) Level curves for constant $|S|$ and $|T|$; (c) Growth of inclination for pure out-of-plane transfer.

or, vice versa, the final inclination is predetermined while the distance is to be maximized (minimized). Since only constant control angles are considered, the problem may be stated mathematically as maximizing the force component $|S|$ as a function of α and β under the constraint that $|T|$ is constant and vice versa. Using Lagrange multipliers, the best control program in both cases is found to satisfy the relation $\cos^2 \alpha \cos^2 \beta = 2/3$. The range of inclinations and distances which can be reached within a given time by these strategies is shown in Figure 5(a). Here the solar parameter ε_s is taken to be 0.15 ($A/m = 100\ \mathrm{m}^2\ (\mathrm{kg})^{-1}$) and the results are valid for any starting radius r_{00} and for outward ($\alpha > 0$) as well as inward ($\alpha < 0$) trajectories. The plot is derived from the analytical values for $i(\nu)$, $r(\nu)$ and $t(\nu)$ involving determination of the response for various values of α and $\beta = \pm \arccos [6^{1/2}/(3 \cos \alpha)]$. The arrows in Figure 5(a) indicate the direction in the γ, i plane taken by a particular control strategy α, β. In the case where the radial distance is prescribed at some final time, the required ratio $|S|/|S|_{\max}$ for a given value of ε_s may be established in conjunction with Figure 4, showing the response for the strategy with $|S| = |S|_{\max}$ (i.e., $|\alpha| = 35.26°$ and $\beta = 0$). The ratio of the value for ε_s corresponding to the desired response and the actual ε_s determines the required $|S|/|S|_{\max}$ with sufficient accuracy. The sail setting α, β yielding the maximum inclination is given by the point of intersection of this particular value of $|S|/|S|_{\max}$ and the curve $\cos^2 \alpha \cos^2 \beta = 2/3$ (i.e., the solid curve in Figure 5(b)). Conversely, if the final inclination is prescribed, the corresponding optimal control programme can be determined as follows. For a given ε_s, the required value for $|T|/|T|_{\max}$ may be taken equal to the ratio of the desired final inclination and the one obtained under the control programme corresponding to $|T|_{\max}$, i.e., $\alpha = 0$, $\beta = \pm 35.26°$. (The behaviour of the inclination under the latter control strategy is shown in Figure 5(c) for a few values of ε_s). The optimal sail setting follows readily from Figure 5(b) as the intersection of this value of $|T|$ and the solid curve.

5. Arbitrary Initial Conditions

In this section, approximate analytical solutions for solar sail trajectories with an arbitrary but fixed sail setting and general initial conditions are developed.

5.1. Short-term approximate solution

By expanding the variables u, l, and $\mathbf{K}$ in terms of a straightforward perturbation series in the small parameter ε_s, an initially valid approximate solution is obtained with the zeroth-order solution representing the unperturbed Kepler ellipse with parameters l_{00}, p_{00} and q_{00}. The first-order equations are solved, yielding the expressions for in-plane perturbations as:

$$l_1(\nu) = 2l_{00}SA_{10}(\nu);$$

$$u_1(\nu) = R(\cos \nu - 1)/l_{00} + S\{\cos \nu[q_{00}B_{12} + p_{00}(A_{12} - A_{10}) + 4A_{11}] + \\ + \sin \nu[p_{00}B_{12} - q_{00}(A_{12} + A_{10}) + 4B_{11}] - 4A_{10}\}/(2l_{00}), \quad (18)$$

where the integrals A_{nk}, B_{nk} for $n = 1, 2, 3, \ldots$ and $k = (0), 1, 2, \ldots$ are defined and evaluated in Appendix I.

It may be noted that for an initially circular orbit, the changes in a, l and r after one revolution are all equal to $4\pi a_{00}S$. The short-term behaviour of the orbital plane expressed in terms of i and ψ is given by

$$\psi(\nu) = \nu - \arctan \frac{T[A_{11}(\nu) \sin \nu - B_{11}(\nu) \cos \nu]}{T[A_{11}(\nu)\cos \nu + B_{11}(\nu) \sin \nu]} + 0(\varepsilon_s^2),$$

$$i(\nu) = |T|[A_{11}^2(\nu) + B_{11}^2(\nu)]^{1/2} + 0(\varepsilon_s^2). \tag{19}$$

This result indicates that after one revolution the position of the ascending node is at $\tilde{\omega}_{00} + \pi + 0(\varepsilon_s^2)$, i.e., near the aphelion, if $T > 0$ and at $\tilde{\omega}_{00} + 0(\varepsilon_s^2)$ (near perihelion) for $T < 0$. This result can be understood physically: although the angular rate of the orbital plane, $W_3 = \varepsilon_s Tu/l^{1/2}$, is smaller near aphelion than that near perihelion, the angular change per radian traversed by the satellite is larger near aphelion since $1/\dot{\nu}$ is proportional to r^2. Hence it is also evident that for an initially circular orbit, the orbital plane returns to its original position after one revolution (in the first-order approximation).

5.2. Long-term behaviour of the elements

A long-term approximate solution for the orbital elements of the solar sail trajectory with fixed sail setting and arbitrary initial conditions can be derived by means of the two-variable expansion procedure (Nayfeh, 1973). Thereto, a new independent slow variable $\bar{\nu} = \varepsilon\nu$ is introduced and the variables u, l and $\mathbf{K}$ are expanded in asymptotic series:

$$u(\nu) = \sum_{n=0}^{N-1} \varepsilon_s^n u_n(\nu, \bar{\nu}) + 0(\varepsilon_s^N);$$

$$l(\nu) = \sum_{n=0}^{N-1} \varepsilon_s^n l_n(\nu, \bar{\nu}) + 0(\varepsilon_s^N);$$

$$\mathbf{K}(\nu) = \sum_{n=0}^{N-1} \varepsilon_s^n \mathbf{K}_n(\nu, \bar{\nu}) + 0(\varepsilon_s^N). \tag{20}$$

Substituting these series into Equations (5) using $\mathrm{d}/\mathrm{d}\nu = \partial/\partial\nu + \varepsilon_s \partial/\partial\bar{\nu}$ and $\mathrm{d}^2/\mathrm{d}\nu^2 = \partial^2/\partial\nu^2 + 2\varepsilon_s \partial^2/(\partial\nu\partial\bar{\nu}) + \varepsilon_s^2 \partial^2/\partial\bar{\nu}^2$, and collecting terms of like powers in ε_s, leads to equations for the subsequent levels of approximation. The zeroth-order equations admit solutions, written as follows:

$$\begin{aligned}
u_0(\nu,\bar{\nu}) &= [1 + p_0(\bar{\nu}) \cos \nu + q_0(\bar{\nu}) \sin \nu]/l_0(\bar{\nu}), & p_0(0) &= p_{00}; \\
& & q_0(0) &= q_{00}; \\
l_0(\nu, \bar{\nu}) &= l_0(\bar{\nu}), & l_0(0) &= l_{00}; \\
M_0(\nu, \bar{\nu}) &= A_0(\bar{\nu}) \cos \nu + B_0(\bar{\nu}) \sin \nu, & A_0(0) &= B_0(0) = 0; \\
K_0(\nu, \bar{\nu}) &= K_0(\bar{\nu}), & K_0(0) &= 1.
\end{aligned} \tag{21}$$

Physically, one can interpret the expression for u_0 as a trajectory tangent to osculating ellipses with slowly varying mean elements. These averaged orbital elements differ from the usual osculating parameters in the sense that short-term periodic variations are disregarded.

The functions p_0, q_0, l_0, A_0, B_0 and K_0 of the slow variable $\bar{\nu}$ are determined from constraints imposed upon the first-order contributions. The equations for the first-order terms become:

$$\frac{\partial^2 u_1}{\partial \nu^2} + u_1 = -2\frac{\partial^2 u_0}{\partial \nu \partial \bar{\nu}} - l_1/l_0^2 - \left(R + S\frac{\partial u_0}{\partial \nu}/u_0\right)/l_0,$$

$$u_1(0) = 0; \quad \frac{\partial u_1}{\partial \nu}(0) = -\frac{\partial u_0}{\partial \bar{\nu}}(0);$$

$$\frac{\partial l_1}{\partial \nu} = -\frac{\mathrm{d}l_0}{\mathrm{d}\bar{\nu}} + 2S/u_0, \qquad l_1(0) = 0;$$

$$\frac{\partial^2 M_1}{\partial \nu^2} + M_1 = -2\frac{\partial^2 M_0}{\partial \nu \partial \bar{\nu}} + TK_0/(u_0 l_0), \quad M_1(0) = 0; \frac{\partial M_1}{\partial \nu}(0) = -\frac{\partial M_0}{\partial \bar{\nu}}(0);$$

$$\frac{\partial K_1}{\partial \nu} = -\frac{\mathrm{d}K_0}{\mathrm{d}\bar{\nu}} - T\frac{\partial M_0}{\partial \nu}/(u_0 l_0), \qquad K_1(0) = 0. \tag{22}$$

In order that the zeroth-order terms remain a valid approximation over a long duration, it is required that the first-order terms do not contain unbounded contributions (in the variable ν). Therefore, the right-hand-sides of Equations (22) are developed in Fourier series with slowly varying coefficients. To eliminate (mixed) secular terms in the solutions for u_1 and M_1, the coefficients of sin ν and cos ν need to vanish, while for suppressing unbounded contributions in l_1 and K_1, the non-harmonic terms must be set equal to zero. This leads to the system of equations:

$$\begin{aligned}
p_0'(\bar{\nu}) &= Sp_0[1 - (1 - e_0^2)^{1/2}]/e_0^2, & p_0(0) &= p_{00};\\
q_0'(\bar{\nu}) &= Sq_0[1 - (1 - e_0^2)^{1/2}]/e_0^2, & q_0(0) &= q_{00};\\
l_0'(\bar{\nu}) &= 2Sl_0/(1 - e_0^2)^{1/2}, & l_0(0) &= l_{00};\\
A_0'(\bar{\nu}) &= TK_0q_0[1/(1 - e_0^2)^{1/2} - 1]/e_0^2, & A_0(0) &= 0;\\
B_0'(\bar{\nu}) &= -TK_0p_0[1/(1 - e_0^2)^{1/2} - 1]/e_0^2, & B_0(0) &= 0;\\
K_0'(\bar{\nu}) &= -T[p_0B_0 - q_0A_0][1/(1 - e_0^2)^{1/2} - 1]/e_0^2, & K_0(0) &= 1.
\end{aligned} \tag{23}$$

It follows from Equations (23) that $\tilde{\omega}_0(\bar{\nu}) = \tilde{\omega}_{00}$ is a constant so that the orientation of the major axis remains fixed in the long run. To analyse the behaviour of the eccentricity, the auxiliary element $w(\bar{\nu}) = 1 - [1 - e^2(\bar{\nu})]^{1/2}$ is introduced and the following equation for w_0 is found from Equations (23)

$$w_0'(\bar{\nu}) = Sw_0/(1 - w_0), \qquad w_0(0) = w_{00}. \tag{24}$$

If $w_{00} = 0$, i.e. initial orbit is circular, it follows that the orbit will remain circular in the long run: $w_0(\bar{\nu}) = e_0(\bar{\nu}) = 0$. It may be noted that $u_0(\nu, \bar{\nu})l_0(\bar{\nu}) = 1$ and

$l_0(\bar{\nu}) = l_{00} \exp(2S\bar{\nu})$ when $e_{00} = 0$ in accordance with the exact spiral solution discussed in Section 2.

For $w_{00} \neq 0$, integration of Equation (24) leads to the following implicit equation for $w_0(\bar{\nu})$,

$$w_0(\bar{\nu}) = w_{00} \exp[S\bar{\nu} + w_0(\bar{\nu}) - w_{00}]. \tag{25}$$

Quite accurate representations for $w_0(\bar{\nu})$ can be established through a process of successive substitution. Initiating the procedure by replacing $w_0(\bar{\nu})$ with $w_0^{(0)} = w_{00}$ in the right-hand-side of Equation (25), subsequent more accurate approximations for $w_0(\bar{\nu})$ follow from:

$$w_0^{(n)}(\bar{\nu}) = w_{00} \exp[S\bar{\nu} + w_0^{(n-1)} - w_{00}], \tag{26}$$

for $n = 1, 2, 3, \ldots$. This iteration scheme converges very rapidly as long as e_{00} is not too close to unity. For small e_{00}, an asymptotic series in terms of powers of w_{00} can be established from the scheme in Equation (26). It can be shown that error term in $w_0^{(n)}(\bar{\nu})$ as an approximation for $w_0(\bar{\nu})$ is of the order w_{00}^{n+1} for $w_{00} \to 0$. For most purposes, the asymptotic expansion of $w_0^{(3)}(\bar{\nu})$ for $w_{00} \to 0$ would provide sufficiently accurate results:

$$\begin{aligned} w_0^{(3)}(\bar{\nu}) = {} & w_{00} \exp(S\bar{\nu}) + w_{00}^2 [\exp(2S\bar{\nu}) - \exp(S\bar{\nu})] + \\ & + w_{00}^3 [3 \exp(3S\bar{\nu}) - 4 \exp(2S\bar{\nu}) + \exp(S\bar{\nu})]/2 + 0(w_{00}^4). \end{aligned} \tag{27}$$

It should be emphasized that a series in terms of powers of w_{00} is more useful than the one in powers of e_{00} for small e_{00}, since $w_{00} = e_{00}^2/2 + 0(e_{00}^4)$ for $e_{00} \to 0$. From the results for $w_0^{(n)}(\bar{\nu})$, Equation (26), the corresponding eccentricity $e_0^{(n)}(\bar{\nu})$ can readily be evaluated from the relation,

$$e_0^{(n)}(\bar{\nu}) = \{1 - [1 - w_0^{(n)}(\bar{\nu})]^2\}^{1/2}, \tag{28}$$

to any desired accuracy by taking n sufficiently large. For small e_{00}, asymptotic series in terms of powers of w_{00} can be derived. The expansion of $e_0^{(3)}(\bar{\nu})$ would serve most needs:

$$\begin{aligned} e_0^{(3)}(\bar{\nu}) = {} & e_{00} \exp(S\bar{\nu}/2)\{1 + w_{00} [\exp(S\bar{\nu}) - 1]/4 + \\ & + w_{00}^2 [3 - 10 \exp(S\bar{\nu}) + 7 \exp(2S\bar{\nu})]/32 + 0(w_{00}^3)\}. \end{aligned} \tag{29}$$

The long-term solutions for $p_0(\bar{\nu})$ and $q_0(\bar{\nu})$ are readily expressed in terms of $e_0(\bar{\nu})$,

$$p_0^{(n)}(\bar{\nu}) = p_{00} e_0^{(n)}(\bar{\nu})/e_{00}, \quad q_0^{(n)}(\bar{\nu}) = q_{00} e_0^{(n)}(\bar{\nu})/e_{00}, \tag{30}$$

and asymptotic series are established using Equation (29).

The attention is focused on the behaviour of the semi-latus rectum. Through Equations (23), $l_0(\bar{\nu})$ can be expressed in terms of $w_0(\bar{\nu})$:

$$l_0(\bar{\nu}) = l_{00} \exp\left\{2S \int_0^{\bar{\nu}} \frac{d\bar{\tau}}{1 - w_0(\bar{\tau})}\right\}. \tag{31}$$

For the first few approximations of $w_0(\bar{\nu})$, the integral can be evaluated explicitly:

$$l_0^{(1)}(\bar{\nu}) = l_{00}(1 - e_{00}^2)\exp(2S\bar{\nu})/[1 - w_{00}\exp(S\bar{\nu})]^2;$$

$$l_0^{(2)}(\bar{\nu}) = l_{00}\left\{\frac{(1 - w_{00})\exp(2S\bar{\nu})}{1 - w_{00}\exp(S\bar{\nu}) + w_{00}^2[\exp(S\bar{\nu}) - \exp(2S\bar{\nu})]}\right\} \times$$

$$\times\left\{\frac{2 + w_{00}[(w_{00}^2 - 2w_{00} + 5)^{1/2} + w_{00} - 1]\exp(S\bar{\nu})}{2 - w_{00}[(w_{00}^2 - 2w_{00} + 5)^{1/2} - w_{00} + 1]\exp(S\bar{\nu})}\right\}^{(1-w_{00})/(w_{00}^2 - 2w_{00} + 5)^{1/2}} \tag{32}$$

However, the following asymptotic representation is more useful for small e_{00}:

$$l_0^{(2)}(\bar{\nu}) = l_{00}\exp(2S\bar{\nu})\{1 + 2w_{00}[\exp(S\bar{\nu}) - 1] + w_{00}^2[4\exp(2S\bar{\nu}) - 6\exp(S\bar{\nu}) + 2] + 0(w_{00}^3)\}. \tag{33}$$

A long-term approximation for the radial distance $r = 1/u$ is given by

$$r_0^{(n)}(\nu, \bar{\nu}) = l_0^{(n)}(\bar{\nu})/[1 + e_0^{(n)}(\bar{\nu})\cos(\nu - \tilde{\omega}_{00})], \tag{34}$$

where the desired representations for $l_0^{(n)}$ and $e_0^{(n)}$ need to be substituted. Also, a long-term approximation for the semi-major axis $a_0(\bar{\nu})$ is known,

$$a_0^{(n)}(\bar{\nu}) = l_0^{(n)}(\bar{\nu})/[1 - w_0^{(n)}(\bar{\nu})]^2. \tag{35}$$

Next, the time history of the satellite in its trajectory is studied. Since $t'(\nu) = r^2/l^{1/2}$, it is obvious that

$$t(\nu) = \int_0^{\nu} l^{3/2}(\bar{\tau})\,\mathrm{d}\tau/[1 + e(\bar{\tau})\cos(\tau - \tilde{\omega}_{00})]^2. \tag{36}$$

Through substitution of $l_0^{(n)}$ and $e_0^{(n)}$ into the integrand, a long-term valid explicit approximation for $t(\nu)$ may be derived. It is more convenient, however, to determine asymptotic series for $t(\nu)$. In this regard, it must be emphasized that, due to the integration of terms depending upon $\bar{\nu}$, a consistent asymptotic series of $t(\nu)$ should be of the form:

$$t(\nu) = t_{-1}(\bar{\nu})/\varepsilon_s + t_0(\nu, \bar{\nu}) + \varepsilon_s t_1(\nu, \bar{\nu}) + 0(\varepsilon_s^2). \tag{37}$$

Substitution of $l_0^{(1)}$ and $e_0^{(1)}$ into Equation (36) and integration leads to the following approximation for $t_{-1}(\bar{\nu})$:

$$t_{-1}^{(1)}(\bar{\nu}) = a_{00}^{3/2}\{[\exp(3S\bar{\nu}) - 1]/3 + e_{00}^2[3\exp(4S\bar{\nu}) - 4\exp(3S\bar{\nu}) + 1]/4 + 0(e_{00}^3)\}/S. \tag{38}$$

It is interesting to note that this result is consistent with the exact spiral solution of Equation (9) when $e_{00} = 0$.

Turning to the long-term behaviour of the orbital plane, it can be seen (from Equations (23)) that the vector $K_0(\bar{\nu}) = (M_0, L_0, K_0)$ traces a path upon a spherical surface: $A_0^2 + B_0^2 + K_0^2 = 1$. Writing $A_0 = C_0 \sin\tilde{\omega}_{00}$ and $B_0 = -C_0\cos\tilde{\omega}_{00}$, an equation for C_0 can be derived and solved,

$$C_0(\bar{\nu}) = \sin\{T[\arcsin e_0(\bar{\nu}) - \arcsin e_{00}]/S\}. \tag{39}$$

Through this expression, all of $M_0(\bar{\nu})$, $L_0(\bar{\nu})$ and $K_0(\bar{\nu})$ can now be written in terms of e_0 and are thus determined up to the required accuracy by substituting the appropriate approximation $e_0^{(n)}(\bar{\nu})$ or its expansions for small e_{00}. The orientation of the orbital plane in terms of the angles ψ_0 and i_0 is given by:

$$\begin{aligned} \psi_0(\bar{\nu}) &= \begin{cases} \tilde{\omega}_{00} + \pi, & T > 0; \\ \tilde{\omega}_{00}, & T < 0; \end{cases} \\ i_0(\bar{\nu}) &= |T|[\arcsin e_0(\bar{\nu}) - \arcsin e_{00}]/S. \end{aligned} \tag{40}$$

5.3. Higher-order contributions

It may be noted that the maximum deviation of the zeroth-order solution from the actual solution is of the order ε_s only for ν up to about $1/\varepsilon_s$. Thus for large values of A/m, higher-order terms may be needed to establish sufficiently accurate long-term approximations.

After incorporating the zeroth-order solutions, the remainder of Equations (22) can be integrated formally, yielding the first-order results:

$$\begin{aligned} u_1(\nu, \bar{\nu}) &= -[R + A_3(\bar{\nu})](1 - \cos \nu)/l_0(\bar{\nu}) + A_2(\bar{\nu}) \cos \nu + B_2(\bar{\nu}) \sin \nu + \\ &\quad + S/l_0(\bar{\nu}) \sum_{j=2}^{\infty} \{[2a_{10}^j/j - p_0 d_{11}^j + q_0 c_{11}^j] \sin (j\nu) - \\ &\quad - [2c_{10}^j/j + p_0 b_{11}^j - q_0 a_{11}^j] \cos (j\nu)\}/(j^2 - 1); \\ l_1(\nu, \bar{\nu}) &= l_0(\bar{\nu}) \left\{ 2S \sum_{j=1}^{\infty} \{a_{10}^j \sin (j\nu) + c_{10}^j [1 - \cos (j\nu)]\}/j + A_3(\bar{\nu}) \right\}; \\ M_1(\nu, \bar{\nu}) &= TK_0(\bar{\nu})(1 - \cos \nu)/(1 - e_{00}^2)^{1/2} + A_4(\bar{\nu}) \cos \nu + B_4(\bar{\nu}) \sin \nu - \\ &\quad - TK_0(\bar{\nu}) \sum_{j=2}^{\infty} \{a_{10}^j \cos (j\nu) + c_{10}^j \sin (j\nu)\}/(j^2 - 1); \\ K_1(\nu, \bar{\nu}) &= T/2 \sum_{j=1}^{\infty} \{[c_{10}^{j+1} - c_{10}^{j-1}] A_0(\bar{\nu}) \sin (j\nu) - [a_{10}^{j+1} - a_{10}^{j-1}] A_0(\bar{\nu}) \times \\ &\quad \times [1 - \cos (j\nu)] - [a_{10}^{j+1} + a_{10}^{j-1}] B_0(\bar{\nu}) \sin (j\nu) - [c_{10}^{j+1} + c_{10}^{j-1}] \times \\ &\quad \times B_0(\bar{\nu})[1 - \cos (j\nu)]\}/j + A_5(\bar{\nu}). \end{aligned} \tag{41}$$

The Fourier coefficients a_{nk}^j, b_{nk}^j, etc., depend on the slow functions $p_0(\bar{\nu})$ and $q_0(\bar{\nu})$ and are evaluated in Appendix II. The functions $A_j(\bar{\nu})$, $B_j(\bar{\nu})$, $j = 2, 3, 4, 5$, are to be determined, as usual, from constraints imposed upon the behaviour of the second-order terms. Equations for these terms can be established by Fourier analysis, leading to lengthy equations for the functions A_j, B_j when eliminating the secular contributions to u_2, l_2, etc. For instance, the least complicated one is given by,

$$\begin{aligned} A_3'(\bar{\nu}) = &-A_3 l_0'/l_0 - S(R + A_3)[a_{20}^0 - a_{21}^0] + S l_0 [A_2 a_{21}^0 + B_2 b_{21}^0] + \\ &+ S^2 \sum_{j=2}^{\infty} \{c_{20}^j [2a_{10}^j/j - p_0 d_{11}^j + q_0 c_{11}^j] - a_{20}^j \times \\ &\times [2c_{10}^j/j + p_0 b_{11}^j - q_0 a_{11}^j]\}, \end{aligned}$$

with all Fourier coefficients depending on $\bar{\nu}$. While analytical solutions have not been found for general eccentricity, in the special case of $e_{00} = 0$ it follows that $e_0(\bar{\nu}) = 0$ and the equations for A_j and B_j can be integrated yielding the following complete first-order solutions:

$$l_1(\bar{\nu}) = 2l_{00}RS\bar{\nu}\exp(2S\bar{\nu});$$

$$e_1(\nu, \bar{\nu}) = \{(R^2 + 4S^2)[1 + \exp(S\bar{\nu}) - 2\exp(S\bar{\nu}/2)\cos\nu]\}^{1/2};$$

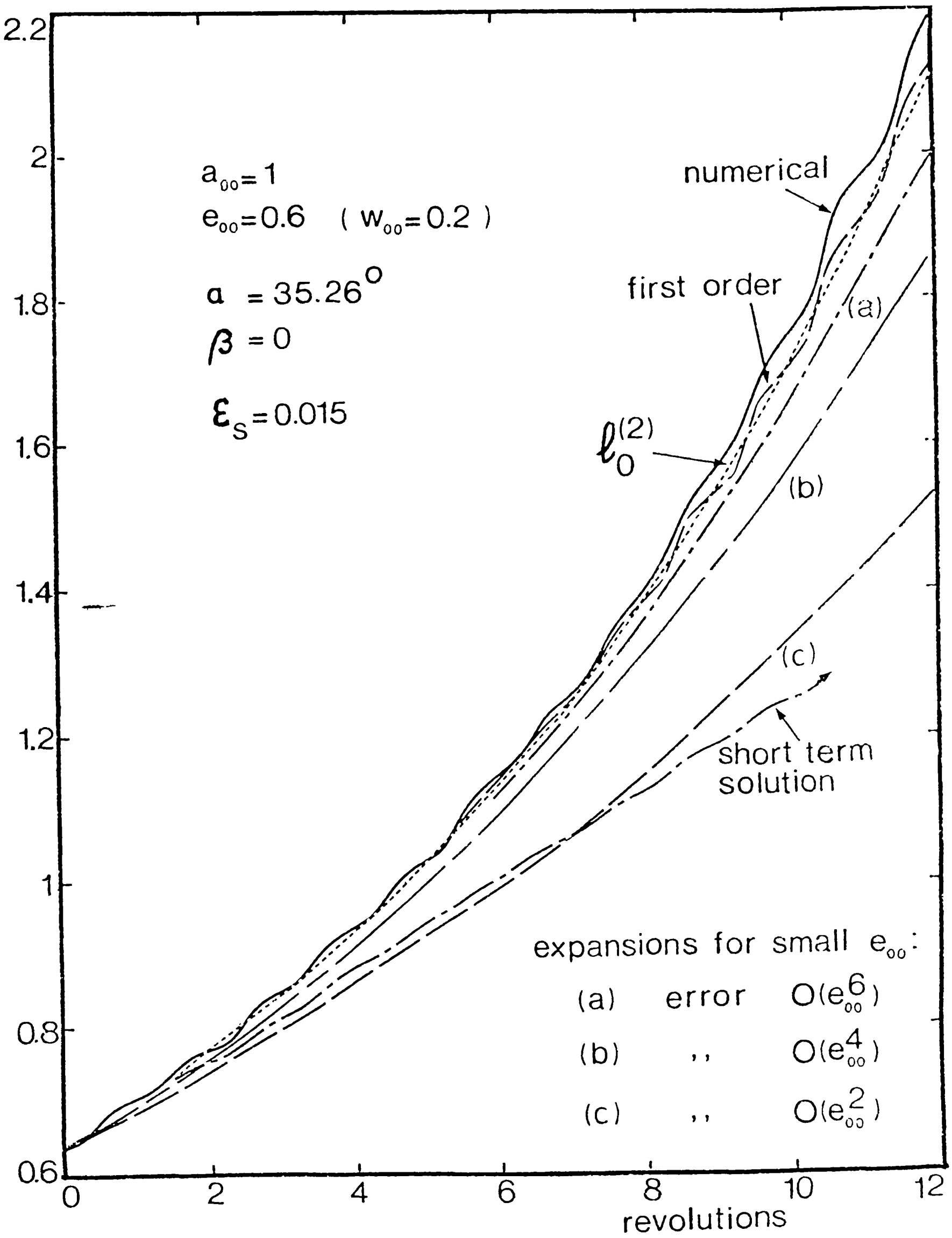

Fig. 6. Comparison of the analytical results for the long-term behaviour of the semi-latus rectum.

$$\tilde{\omega}_1(\nu, \bar{\nu}) = \arctan\left\{\frac{2S[\exp(S\bar{\nu}/2) - \cos\nu] - R\sin\nu}{R[\exp(S\bar{\nu}/2) - \cos\nu] + 2S\sin\nu}\right\};$$

$$r(\nu, \bar{\nu}) = l_{00}\exp(2S\bar{\nu})\{1 + \varepsilon_s R[1 - \exp(S\bar{\nu}/2)\cos\nu] - 2\varepsilon_s S\exp(S\bar{\nu}/2)\sin\nu\} + 0(\varepsilon_s^2). \quad (42)$$

It is seen that the radial distance oscillates around the spiral solution $r = l_{00}\exp(2S\bar{\nu})$ with slowly increasing amplitude of oscillation.

As to the orientation of the orbital plane, it follows that

$$\psi(\nu, \bar{\nu}) = \nu - \arctan\left\{\frac{S(1 - \cos\nu) + [2S\cos\nu - R\sin\nu][\exp(S\bar{\nu}/2) - 1]}{S\sin\nu - [2S\sin\nu + R\cos\nu][\exp(S\bar{\nu}/2) - 1]}\right\} + 0(\varepsilon_s^2);$$

$$i(\nu, \bar{\nu}) = \varepsilon_s|T|/S\{(4S^2 + R^2)[\exp(S\bar{\nu}/2) - 1]^2 + 4S^2(\cos\nu - 1) \times [\exp(S\bar{\nu}/2) - 3/2] - 2RS\sin\nu\,[\exp(S\bar{\nu}/2) - 1]\} + 0(\varepsilon_s^2). \quad (43)$$

These results illustrate that the amplitude of the perturbations grows slowly.

5.4. Discussion of results

In order to assess the relative accuracies of the approximate results, comparisons are made with a numerical solution of the exact Equations (5) using a double-precision Runge–Kutta integration routine. The high value of initial eccentricity ($e_{00} = 0.6$) is chosen to illustrate a rather extreme situation, while ε_s is taken to be 0.015. Figure 6 shows the various approximations for the semi-latus rectum: obviously, the short-term solution has a limited range of validity, while the near-circular expansions of

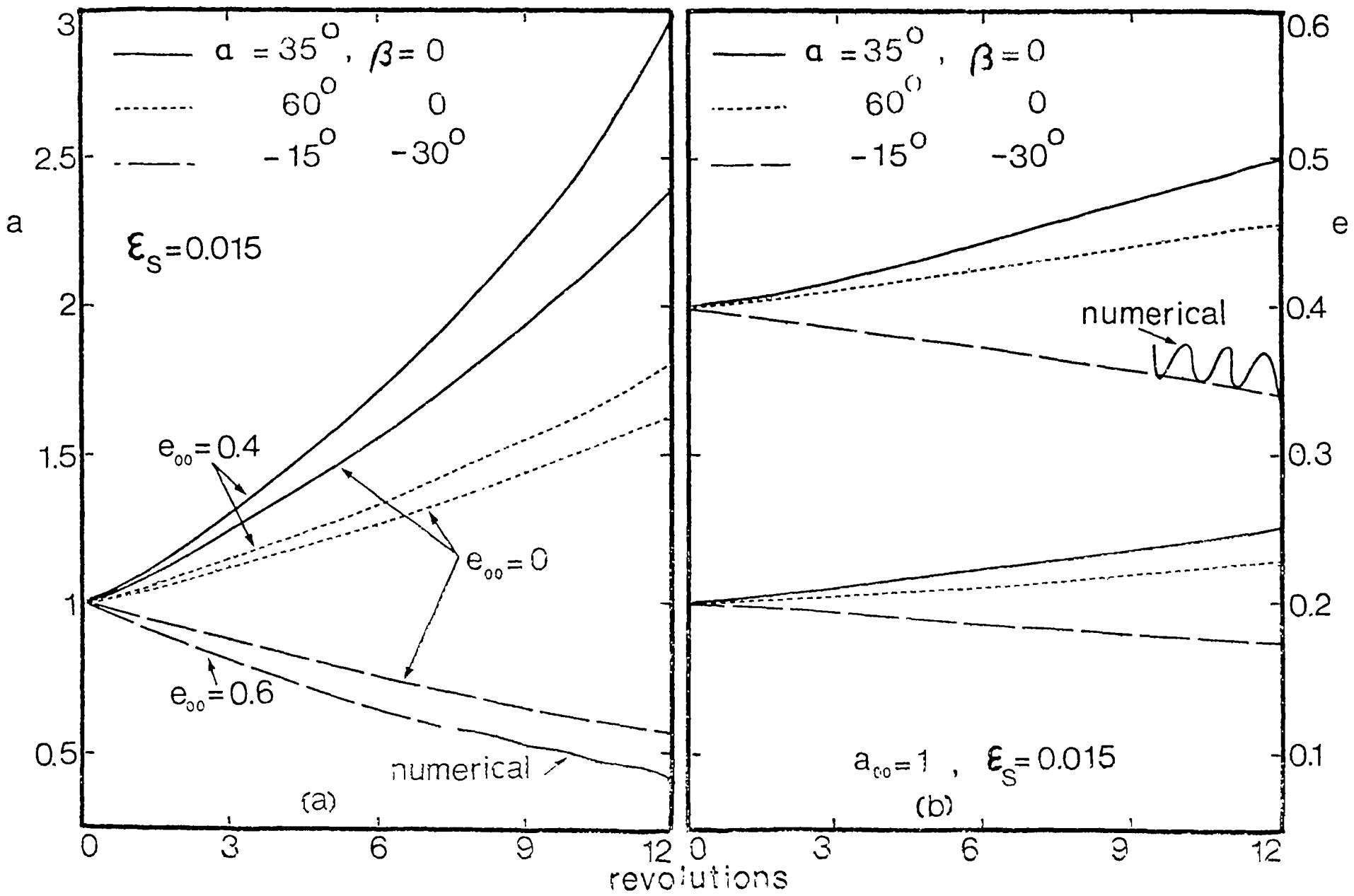

Fig. 7. Long-term behaviour of semi-major axis and eccentricity as predicted by the zeroth-order solution.

$l_0^{(1)}$ and $l_0^{(2)}$ may give fairly accurate long-term approximations provided a sufficient number of terms are retained for high values of e_{00} (curve a). The solution $l_0^{(2)}$ is more accurate, naturally, and would be the most appropriate candidate for predicting long-term, high-eccentricity trends. The effect of the first-order contributions, $l_1(\nu, \bar{\nu})$ from Equations (41) is added to $l_0^{(2)}$ illustrating the small-amplitude oscillations around the mean trend designated by $l_0^{(2)}$ itself. The slow function $A_3(\bar{\nu})$ was taken to be zero throughout. The discrepancy between the numerical solution and this (best) analytical approximation is largely due to the effect of $A_3(\bar{\nu})$. Other contributions to the error may be attributed to the fact that $l_0^{(2)}$ represents an approximation for $l_0(\bar{\nu})$ and the higher-order terms are neglected.

Figure 7(a) shows the long-term trend of the semi-major axis for a few sail settings. The approximation $a_0^{(2)}(\bar{\nu})$ compares quite well with the exact numerical solution: at least to two significant digits over the first 12 revolutions. The long-term behaviour of eccentricity is depicted in Figure 7(b), where the approximation $e_0^{(2)}(\bar{\nu})$ was used. Relatively large first-order contributions separate the zeroth-order approximations from the exact solutions in this case. Nevertheless, the qualitative trend of the long-term behaviour of the eccentricity is predicted correctly.

6. Concluding Remarks

The results of the present paper can be summarized in the form of the following general conclusions:

(i) An exact three-dimensional solution in the form of a logarithmic spiral is presented for certain specific initial conditions by separating the out-of-plane and in-plane motions.

(ii) An effective near-circular, out-of-plane spiral transfer trajectory has been explored in detail permitting any combination of final radial distance and orbital inclination.

(iii) Short- as well as long-term approximate solutions have been established for arbitrary initial conditions. For small initial eccentricity, asymptotic series for the orbital elements should prove useful for long-term trajectory evaluation.

Appendix I: Evaluation of the Integrals A_{nk} and B_{nk}

The integrals A_{nk} and B_{nk} are defined as

$$A_{nk}(\nu) = \int_0^{\nu} \cos(k\tau)\, d\tau/(1 + p\cos\tau + q\sin\tau)^n,$$

$$B_{nk}(\nu) = \int_0^{\nu} \sin(k\tau)\, d\tau/(1 + p\cos\tau + q\sin\tau)^n, \tag{I.1}$$

for $k = (0), 1, 2, \ldots; n = 1, 2, 3, \ldots$. The parameters p and q represent the initial

conditions p_{00} and q_{00} or the slow functions $p_0(\bar{\nu})$ and $q_0(\bar{\nu})$. While the integral A_{10} can be evaluated by elementary means, the integrals A_{n0} for higher values of n can be obtained from A_{10} by repeated differentiation within the integrand,

$$A_{10}(\nu) = 2 \arctan \left\{ \frac{(1 - e^2)^{1/2} \tan (\nu/2)}{1 + p + q \tan (\nu/2)} \right\} / (1 - e^2)^{1/2},$$

$$A_{20}(\nu) = \{A_{10}(\nu) - \Psi(\nu)/[1 + \Phi(\nu)] - q/(1 + p)\}/(1 - e^2), \quad \text{etc.} \qquad \text{(I.2)}$$

where $\Phi(\nu)$ and $\Psi(\nu)$ denote $p \cos \nu + q \sin \nu$ and $p \sin \nu - q \cos \nu$ respectively.

The integrals with $n \leqslant k$ can usually be determined quite readily:

$$A_{11}(\nu) \left\{ = p[\nu - A_{10}(\nu)] + q \ln \left| \frac{1 + \Phi(\nu)}{1 + p} \right| \right\} / e^2;$$

$$B_{11}(\nu) = \left\{ q[\nu - A_{10}(\nu)] - p \ln \left| \frac{1 + \Phi(\nu)}{1 + p} \right| \right\} / e^2;$$

$$A_{12}(\nu) = -2[q + \Psi(\nu)]/e^2 - (p^2 - q^2)[(2 - e^2)A_{10}(\nu)\, 2\nu]/e^4$$
$$- 4pq \ln \left| \frac{1 + \Phi(\nu)}{1 + p} \right| / e^4;$$

$$B_{12}(\nu) = 2[p - \Phi(\nu)]/e^2 + 2pq[(2 - e^2)A_{10}(\nu) - 2\nu]/e^4 -$$
$$- 2(p^2 - q^2) \ln \left| \frac{1 + \Phi(\nu)}{1 + p} \right| / e^4. \qquad \text{(I.3)}$$

These results are not suited for $e \to 0$, and are to be replaced by:

$$A_{11}(\nu) = -p\nu/2 + [1 + 3p^2/4 + q^2/4] \sin \nu - p \sin (2\nu)/4 +$$
$$+ pq(1 - \cos \nu)/2 - q[1 - \cos (2\nu)]/4 + (p^2 - q^2) \sin (3\nu)/12 +$$
$$+ pq[1 - \cos (3\nu)]/6 + 0(e^3);$$

$$B_{11}(\nu) = -q\nu/2 + pq \sin \nu/2 + [1 + p^2/4 + 3q^2/4](1 - \cos \nu) +$$
$$+ q \sin (2\nu)/4 - p[1 - \cos (2\nu)]/4 - pq \sin (3\nu)/6 +$$
$$+ (p^2 - q^2)[1 - \cos (3)]/12 + 0(e^3);$$

$$A_{12}(\nu) = \sin (2\nu)/2 - p/2 \sin \nu + q(1 - \cos \nu)/2 - p \sin (3\nu)/6 -$$
$$- q[1 - \cos (3\nu)]/6 + 0(e^2); \qquad \text{(I.4)}$$

$$B_{12}(\nu) = [1 - \cos (2\nu)]/2 - q/2 \sin \nu + p(1 - \cos \nu)/2 + q \sin (3\nu)/6 -$$
$$- p[1 - \cos (3\nu)]/6 + 0(e^2).$$

Appendix II: Evaluation of the Fourier coefficients $a^j_{nk}, \ldots, d^j_{nk}$

The Fourier coefficients of the functions

$$\cos (k\nu)/[1 + p \cos \nu + q \sin \nu]^n = a^0_{nk}/2 + \sum_{j=1}^{\infty} \{a^j_{nk} \cos j\nu + c^j_{nk} \sin j\nu\},$$

$$\sin (k\nu)/[1 + p \cos \nu + q \sin \nu]^n = b^0_{nk}/2 + \sum_{j=1}^{\infty} \{b^j_{nk} \cos j\nu + d^j_{nk} \sin j\nu\},$$

(II.1

for $k = (0), 1, 2, \ldots$ and $n = 1, 2, 3, \ldots$ can be expressed in terms of the integrals $A_{nk}(2\pi)$ and $B_{nk}(2\pi)$ as follows:

$$a_{nk}^{j} = \frac{1}{\pi}\int_{0}^{2\pi} \frac{\cos(k\tau)\cos(j\tau)\,\mathrm{d}\tau}{(1 + p\cos\tau + q\sin\tau)^{n}} = [A_{n,j+k}(2\pi) + A_{n,j-k}(2\pi)]/(2\pi);$$

$$b_{nk}^{j} = \frac{1}{\pi}\int_{0}^{2\pi} \frac{\sin(k\tau)\cos(j\tau)\,\mathrm{d}\tau}{(1 + p\cos\tau + q\sin\tau)^{n}} = [B_{n,j+k}(2\pi) - B_{n,j-k}(2\pi)]/(2\pi);$$

$$c_{nk}^{j} = \frac{1}{\pi}\int_{0}^{2\pi} \frac{\cos(k\tau)\sin(j\tau)\,\mathrm{d}\tau}{(1 + p\cos\tau + q\sin\tau)^{n}} = [B_{n,j-k}(2\pi) + B_{n,j+k}(2\pi)]/(2\pi);$$

$$d_{nk}^{j} = \frac{1}{\pi}\int_{0}^{2\pi} \frac{\sin(k\tau)\sin(j\tau)\,\mathrm{d}\tau}{(1 + p\cos\tau + q\sin\tau)^{n}} = [A_{n,j-k}(2\pi) - A_{n,j+k}(2\pi)]/(2\pi). \tag{II.2}$$

It may be noted that $A_{n,j-k} = A_{n,k-j}$ and $B_{n,j-k} = -B_{n,k-j}$.
The following explicit expressions for the Fourier coefficients can be derived:

$$\begin{pmatrix} a_{1\,0}^{j} \\ c_{1\,0}^{j} \end{pmatrix} = 2\begin{pmatrix} \cos(j\omega) \\ \sin(j\omega) \end{pmatrix}[(1-e^2)^{1/2} - 1]^{j} e^{-j}/(1-e^2)^{1/2};$$

$$\begin{pmatrix} a_{2\,0}^{j} \\ c_{2\,0}^{j} \end{pmatrix} = 2\begin{pmatrix} \cos(j\omega) \\ \sin(j\omega) \end{pmatrix}[(1-e^2)^{1/2} - 1]^{j}[1 + j(1-e^2)^{1/2}]e^{-j}/(1-e^2)^{3/2};$$

$$\begin{pmatrix} a_{3\,0}^{j} \\ c_{3\,0}^{j} \end{pmatrix} = \frac{[(1-e^2)^{1/2} - 1]^{j}}{e^{j}(1-e^2)^{5/2}}\begin{pmatrix} \cos(j\omega) \\ \sin(j\omega) \end{pmatrix}[2 + e^2 + 3j(1-e^2)^{1/2} + j^2(1-e^2)];$$

$$\begin{pmatrix} a_{1\,1}^{j} \\ c_{1\,1}^{j} \end{pmatrix} = -\frac{2[(1-e^2)^{1/2} - 1]^{j}}{e^{j+1}}\left\{\frac{\cos\omega}{(1-e^2)^{1/2}}\begin{pmatrix} \cos(j\omega) \\ \sin(j\omega) \end{pmatrix} + \sin\omega\begin{pmatrix} \sin(j\omega) \\ -\cos(j\omega) \end{pmatrix}\right\};$$

$$\begin{pmatrix} b_{1\,1}^{j} \\ d_{1\,1}^{j} \end{pmatrix} = -\frac{2[(1-e^2)^{1/2} - 1]^{j}}{e^{j+1}}\left\{\frac{\sin\omega}{(1-e^2)^{1/2}}\begin{pmatrix} \cos(j\omega) \\ \sin(j\omega) \end{pmatrix} + \cos\omega\begin{pmatrix} -\sin(j\omega) \\ \cos(j\omega) \end{pmatrix}\right\};$$

$$\begin{pmatrix} a_{2\,1}^{j} \\ c_{2\,1}^{j} \end{pmatrix} = -\frac{2[(1-e^2)^{1/2} - 1]^{j}}{e^{j+1}(1-e^2)^{3/2}}\left\{[e^2 + j(1-e^2)^{1/2}]\cos\omega\begin{pmatrix} \cos(j\omega) \\ \sin(j\omega) \end{pmatrix} + \right.$$

$$\left. + j(1-e^2)\sin\omega\begin{pmatrix} \sin(j\omega) \\ -\cos(j\omega) \end{pmatrix}\right\};$$

$$\begin{pmatrix} b_{2\,1}^{j} \\ d_{2\,1}^{j} \end{pmatrix} = -\frac{2[(1-e^2)^{1/2} - 1]^{j}}{e^{j+1}(1-e^2)^{3/2}}\left\{[e^2 + j(1-e^2)^{1/2}]\sin\omega\begin{pmatrix} \cos(j\omega) \\ \sin(j\omega) \end{pmatrix} + \right.$$

$$\left. + j(1-e^2)\cos\omega\begin{pmatrix} -\sin(j\omega) \\ \cos(j\omega) \end{pmatrix}\right\};$$

$$\begin{pmatrix} a_{3\,1}^{j} \\ c_{3\,1}^{j} \end{pmatrix} = -\frac{[(1-e^2)^{1/2}-1]^j}{e^{j+1}(1-e^2)^{5/2}}\Big\{[3e^2 + j(1+2e^2)(1-e^2)^{1/2} + j^2(1-e^2)] \times$$

$$\times \cos\omega \begin{pmatrix} \cos(j\omega) \\ \sin(j\omega) \end{pmatrix} + j(1-e^2)[1+j(1-e^2)^{1/2}] \sin\omega \begin{pmatrix} \sin(j\omega) \\ -\cos(j\omega) \end{pmatrix}\Big\};$$

$$\begin{pmatrix} b_{3\,1}^{j} \\ \mathrm{d}_{3\,1}^{j} \end{pmatrix} = -\frac{[(1-e^2)^{1/2}-1]^j}{e^{j+1}(1-e^2)^{5/2}}\Big\{[3e^2 + j(1+2e^2)(1-e^2)^{1/2} + j^2(1-e^2)] \times$$

$$\times \sin\omega \begin{pmatrix} \cos(j\omega) \\ \sin(j\omega) \end{pmatrix} + j(1-e^2)[1+j(1-e^2)^{1/2}] \cos\omega \times$$

$$\times \begin{pmatrix} -\sin(j\omega) \\ \cos(j\omega) \end{pmatrix}\Big\}. \qquad \text{(II.3)}$$

The coefficients $a_{n\,1}^{0}$, b_{n1}^{0} are equal to $a_{n\,0}^{1}$, $b_{n\,0}^{1}$ respectively. For values of k larger than 1, the dominant coefficients can be expressed in terms of the results of Equations (II.3):

$$a_{nk}^{j} = a_{nj}^{k}; \ldots; \quad d_{nk}^{j} = d_{nj}^{k}; \quad j = 0, 1, 2, \ldots \qquad \text{(II.4)}$$

References

Kiefer, J. W.: 1965, *Proceedings of the 15th International Astronautical Congress of the I.A.F.*, Gauthier-Villars, pp. 383–416.

London, H. S.: 1960, *ARS Journal* **30**, 198–200.

Modi, V. J., Pande, K. C., and Nicks, G. W.: 1973, *Proceedings of the 10th International Symposium on Space Technology and Science*, AGNE Publishing Company, pp. 375–382.

Nayfeh, A. J.: 1973, *Perturbation Methods*, Wiley, Ch. 6.

Pozzi, A. and De Socio, L.: 1961, *ARS Journal* **31**, 422–427.

Tsu, T. C.: 1959, *ARS Journal* **29**, 422–427.

Van der Ha, J. C. and Modi, V. J.: 1977, *Acta Astronautica* **4**, 813–831

Wesseling, P.: 1967, *Astronautica Acta* **13**, 431–440.